https://doi.org/10.59761/RCR5080

Influence of surface groups on the properties of disperse systems

Yury M Volfkovich

A.N.Frumkin Institute of Physical Chemistry and Electrochemistry, Russian Academy of Sciences, Leninskii prosp. 31, 119991 Moscow, Russian Federation

Published data on the influence of surface groups on various properties of disperse systems are integrated and analyzed. The preparation of these systems is considered in relation to activated carbon. The discussion addresses the effect of redox reactions of surface groups on the energy efficiency of electrochemical supercapacitors, operation of capacitive deionization units for water desalination, and functioning of redox capacitors based on organic monomers. It is shown that very high energy and power characteristics of lithium ion capacitors are based on the redox reactions of lithium-containing surface groups of highly dispersed graphene electrodes. The effect of surface groups on the self-discharge of electrochemical supercapacitors with activated carbon-based electrodes is demonstrated. The prospects for the production of drinking water by capacitive deionization using mosaic cation/anion exchange membranes are evaluated. The practically important inversion of sulfo groups relative to the polymer chain in the catalyst layers of fuel cells with proton exchange membranes is noted.

The bibliography includes 181 references.

Keywords: activated carbon, electrochemical supercapacitor, surface groups, surface conductivity, capacitive deionization of water, fuel cells.

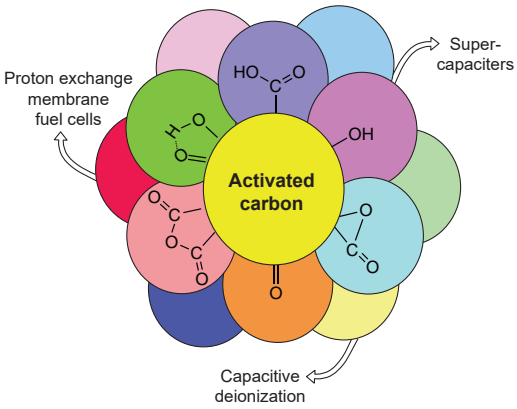

Contents

1. Introduction

Disperse systems are used in scientific research, technology, and industrial processes. Various types of disperse systems include highly dispersed carbon materials [activated carbon (AC), aerogels, graphenes, carbon nanotubes, *etc.*],[1–5] ion exchange membranes, and various composites. Disperse systems form the basis of electrodes in chemical current sources,[6,7] ion-exchange membranes,[8] and active layers of fuel cells.[5,9,10]

Surface groups (SGs),[†] which are present in many disperse systems, considerably influence their functional properties. The presence of SGs imparts some new properties to dispersed materials. For example, AC-based electrodes provide a noticeable conductivity even in pure water.

The demand for highly dispersed carbon materials such as AC characterized by high sorption capacity increases with the progress of industry. Activated carbon is universally used in environmental engineering (for water conditioning and as a part of filters for air and gas purification), in medicine (for haemodialysis), in food industry (to improve the colour, taste, and odour of foodstuffs), and in many other fields. A unique

Yu.M.Volfkovich. Doctor of Chemical Sciences, Chief Researcher at IPCE RAS.
E-mail: yuvolf40@mail.ru
Current research interests: electrochemical energy generation (supercapacitors, fuel cells, batteries), water desalination by capacitive deionization, porosimetry.

[†] It should be noted that the notion ‘surface groups’ is used in publications of many authors, who, however, do not give a strict definition to this term. As applied to the subject matter of this review, we can propose the following definition: ‘surface groups are chemical compounds strongly bound to the surface of highly dispersed materials’.

Received 6 March 2023

feature of AC that is especially valuable for electrochemical applications is that AC is simultaneously an electron and ion exchanger due to electronic conductivity and the presence of numerous surface groups.

Activated carbon is widely used as an electrode material for energy storage devices such as electrochemical supercapacitors (ECSCs). These devices function due to charge separation, which is reversible; therefore ECSCs can rapidly give off energy. Devices similar to supercapacitors are utilized for the capacitive deionization (CDI) of water, which is the most economical and efficient method for desalination and purification of seawater and process water.[8,11–18] The use of AC provides water desalination level that complies with specification requirements in water treatment. The presence of particular SGs in the electrodes has a pronounced effect on the ECSC characteristics and on the CDI process.

Most of electrical energy in all countries is still generated upon combustion of fossil hydrocarbons. However, this is fraught with adverse environmental consequences. Today, it is impossible to overcome this situation using renewable energy sources because of their drawbacks, the main of which are low efficiency of the production units using renewable materials and the possibility of their functioning under definite environmental conditions.

Apparently, the energy supply problem could be solved using fuel cells. These devices with a high overall efficiency are characterized by simple design and environmental friendliness (there are almost no hazardous emissions to the environment). The proton exchange membrane fuel cells (PEMFC) are most widely encountered and most efficient. The structural and hydrophilic — hydrophobic properties of carbon supports in the catalytic layer are determined by the presence of SGs.

The structure of this review reflects the results of research on the influence of SGs on the characteristics of the above-mentioned objects: the preparation methods and studies of properties are considered in relation to AC (Section 2); the effects of SGs on the operation of ECSCs (Section 3), on CDI processes (Section 4), and on the functioning of PEMFC (Section 5) are demonstrated

2. Activated carbon

2.1. Main properties of activated carbon

Activated carbon is a porous substance obtained from various carbon-containing materials of organic origin: charcoal and hard coal, petroleum coke, nutshells and kernels, and also from synthetic polymers (*e.g.*, polyacrylonitrile and polyvinyl chloride). The following unique properties are inherent in AC: large specific surface area (ranging from ~500 to 2500 $m^2\ g^{-1}$),[19–26] clear-cut adsorption capacity,[21–26] electronic conductivity, and the presence of numerous surface groups.[9,12] High specific surface area and high electronic conductivity account for wide use of AC in electrodes for electrochemical devices [24,27–35] and for CDI processes.[36–46]

The key properties and the pore structure of activated carbon are determined, first of all, by the type of the initial carbon raw material and the method of its processing. Activated carbon is produced using various types of industrial furnaces and fluidized-bed reactors. The AC production process includes the following key stages: raw material particles are crushed down to the 3–5 cm size, then carbonized, and then activated.[23,26,45,46] During carbonization, which consists in the pyrolytic decomposition of the starting compound at 500–600 °C, all volatile elements except for carbon (hydrogen, oxygen, nitrogen, *etc*.) are removed.‡ This affords the basis for the future activated carbon, that is, the primary porosity.§ However, the sizes of the pores thus formed (and, hence, the specific surface area) are moderate; therefore, the resulting carbonized material has poor adsorption properties.

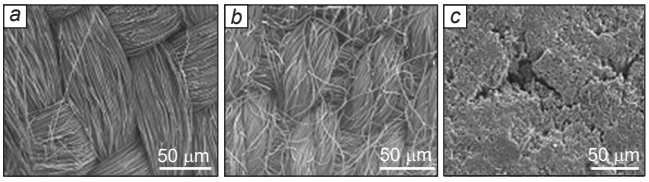

Fig. 1. SEM images of activated carbon materials: VISKUMAK (*a*), CH900 (*b*), and SAIT (*c*). In Fig. *a* and *b*, fibres can be seen, and in Fig. *c*, a composite structure incorporating AC and PTFE particles can be traced.[47]

The activation is carried out to generate a specific pore structure and to enhance the adsorption properties. This is accomplished either by preliminary impregnation of the carbonized material with a solution of zinc chloride, potassium carbonate, or another salt followed by heating to 400–600 °C without access of air or by the most popular method consisting in the oxidation of the carbonized material on treatment with superheated steam, carbon dioxide, or oxygen (or their mixture) at a temperature of 700–900 °C under strictly controlled conditions.

During activation, a part of carbon is removed from the carbonized material, being replaced by pores with linear dimensions ranging from <1 nm to 100 nm. As an example giving an idea of the surface structure of disperse systems, Fig. 1 shows the scanning electron microscopy (SEM) images of carbon-based materials: AC fabrics manufactured under brand names VISKUMAK and CH900 and an AC-based composite SAIT+5% polytetrafluoroethylene (PTFE).

2.2. Study of the structure of activated carbon

The standard contact porosimetry (SCP) method,[48–51] recommended by IUPAC,[52] is a versatile method for studying the porous structure of solids, including disperse systems with a very broad range of linear pore sizes (from ~1 to 10^5 nm). The need for the development of SCP method was caused by the drawbacks and limitations of conventional porosimetry techniques such as mercury intrusion method, centrifugal porosimetry, liquid intrusion porosimetry, capillary condensation, small-angle X-ray scattering, electronic, tunnelling, and atomic force spectroscopy, and optical and microscopic examinations. The major drawback of the first-mentioned method are the toxicity of mercury, deformation and destruction of samples under high pressure, distortion of the results due to amalgamation of most metals, and complexity of the equipment. Other methods are characterized by narrow ranges of measurable linear dimensions of pores (most often, ~1

‡ If necessary (in particular, before being used as parts of electrodes in electrochemical devices), the carbon material obtained after pyrolysis is subjected to acid treatment to remove the remaining non-volatile elements such as silicon, calcium, magnesium, iron, *etc*.

§ The pores in activated carbon are classified in terms of their linear dimension (x): the half-width for the slit-like model or the radius for the cylindrical and spherical models. According to the IUPAC recommendations, micro- ($x<2$ nm), meso- (x ranging from 2 to 50 nm), and macropores ($x>50$ nm) are distinguished.

to 50 nm), difficult sample preparation procedures, and complicated quantitative interpretation of the results.

The method of SCP is free from the above drawbacks. When octane is used as the measuring liquid, the procedure gives porosimetry curves for all pores, while the use of water gives the curves only for hydrophilic pores. Figure 2 shows the integral and differential effective radius distribution of pores for all AC materials

$$r^* = \frac{r}{\cos\theta} \quad (1)$$

(r^* and r are the effective and true pore radius, respectively; q is the contact angle for water), while Fig. 3 depicts the dependence of θ on r^*. Octane wets all materials almost perfectly; therefore, for octane, $\theta \approx 0$ and $r^* \approx r$, while for water, $\theta > 0$ and $r^* > r$.

It can be seen that all AC materials contain both hydrophilic and hydrophobic pores with linear dimensions varying over a very wide range, from fractions of a nanometre to 100 mm, *i.e.*, over a range covering more than five orders of magnitude. The very complex pattern of dependences shown in Fig. 3 is attributable to the non-uniform distribution of hydrophilic SGs

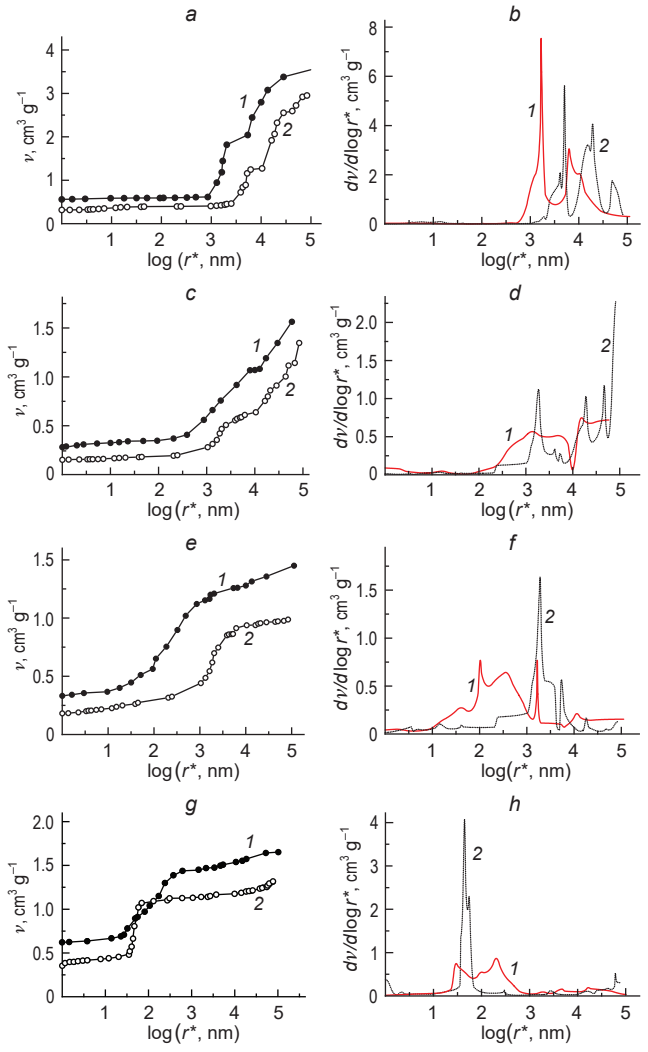

Fig. 2. Integral (*a*, *c*, *e*, *g*) and differential (*b*, *d*, *f*, *h*) porosimetric curves for activated carbon materials: CH900 (*a*, *b*), VISKUMAK (*c*, *d*), SAIT (*e*, *f*), and RIKON (*g*, *h*) measured using octane (*1*) and water (*2*); *v* is the specific pore volume; RIKON is a material based on Norit AC with 4% PTFE binder.[47]

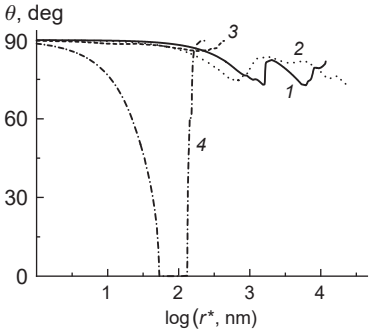

Fig. 3. Dependences of θ on r* for activated carbon materials: CH900 (*1*) VISKUMAK (*2*), SAIT (*3*), and RIKON (*4*). Water was used as the measuring liquid.[47]

in the pores of different size in AC and to the presence of hydrophobic PTFE particles in the RIKON and SAIT materials.

The authors of some publications (see, *e.g.*, Refs 53–64) consider it advantageous to use ACs with a hierarchical pore structure, which is formed upon agglomeration of particles with different size ranges. Many specialists believe that a large specific surface area is the most important characteristic of the pore structure determining the properties of electrodes in electrochemical devices.[65–77]

2.3. Surface conductivity

A general procedure for measuring the surface ionic conductivity of porous electrodes was first reported by Volfkovich *et al.*[78] The concentration and composition of SGs were determined by the standardized Boehm titration for carbon materials.[79–82]

It is known that activated carbon contains numerous surface groups.[83–85] Nitrogen- and oxygen-containing groups are encountered most often (Fig. 4). A study of AG-3 and SKT-6a activated carbons showed the presence of numerous basic groups on their surface (695 and 1402 mmol g^{-1}) and the absence of phenolic groups.[47] It was noted above that SGs have a pronounced effect on the AC properties. Activated carbons possess electronic conductivity, while SG counter-ions provide also the surface ionic conductivity; in other words, AC is both an electron and an ion exchanger. According to M. Smolukhovsky,[82] an electrolyte solution contained in the diaphragm pores has a higher electrical conductivity than the equilibrium solution. The additional, or surface conductivity (SC) is due to the mobility of excess ions of the electric double layer (EDL). The electrical conductivity of the solution in the pores (κ) is the sum of the electrical conductivity of the free equilibrium solution (κ_V) and the surface conductivity. Thus, SC is the longitudinal (tangential) conductivity of EDL. In turn, the surface conductivity is equal to the sum

$$\kappa_{sc} = \kappa_{sg} + \kappa_{sch} \quad (2)$$

where κ_{sg} is the conductivity of the SG counter-ions, while κ_{sch} is the conductivity of SGs depending on their electrostatic charge, caused by the presence of EDL.[84] The κ_{sg} value depends on the SG concentration, that is, on the SG exchange capacity, while κ_{sch} depends on the potential and on the solution concentration.

The relationship of the mentioned values is demonstrated below in relation to the CH900 and SAIT AC materials and for the use of a KCl solution. The *k* values plotted against the KCl concentration for electrodes based on CH900 and SAIT at their stationary potentials are depicted in Fig. 5. It can be seen that at very low concentrations the plots are linear. The κ_{sg} values were determined by extrapolating the presented data to a zero concentration of KCl.[83] The stationary potentials (E_{stat}), the conductivity of counter-ions (κ_{sg}), and the exchange capacity of

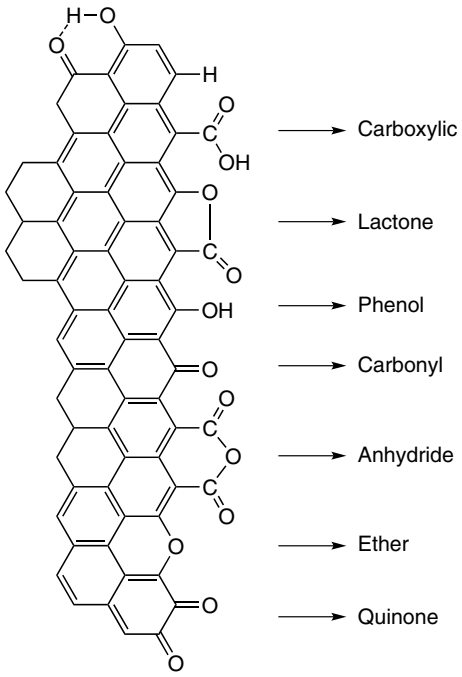

Fig. 4. Examples of surface groups in activated carbon materials.[85]

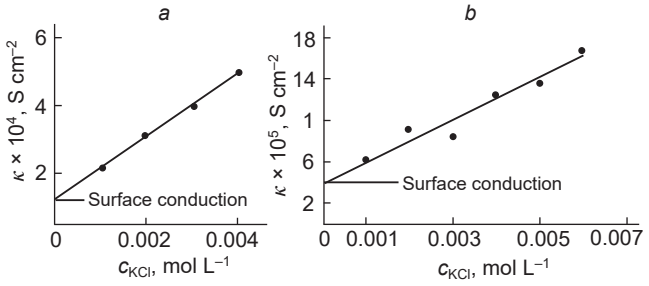

Fig. 5. Electrical conductivity plotted *vs.* concentration of a KCl solution for CH900 (*a*) and SAIT (*b*) electrodes at their stationary potentials.[78]

SGs with respect to the potassium ion (Q) for the indicated electrodes are given below.[45]

Parameter	Q, mg-equiv. g^{-1}	E_{stat}, V	κ_{sg}, S cm^{-1}
CH900	1.14	0.497	0.000123
SAIT	0.37	0.482	0.00004

It follows from the presented data that the Q and κ_{sg} ratios for the CH900 and SAIT electrodes are approximately equal. Hence, the conductivity of counter-ions is roughly proportional to the exchange capacity of SGs

$$\kappa_{sg} \approx Q\kappa_{sgi} \qquad (3)$$

where κ_{sgi} is the surface conductivity for unit exchange capacity (Q=1 mg-equiv. g^{-1}).

The dependences of conductivity on the potential (E) at various KCl concentrations for the considered electrodes are shown in Fig. 6. The E values at the minima of the curves correspond to the total zero charge potential (ZCP). The ranges of variation of this parameter for various carbon materials (in particular, for AC) are very broad: the lowest and highest values can differ by approximately an order of magnitude. The ZCP values found for the given electrodes are in line with the published data. Thus, the method for

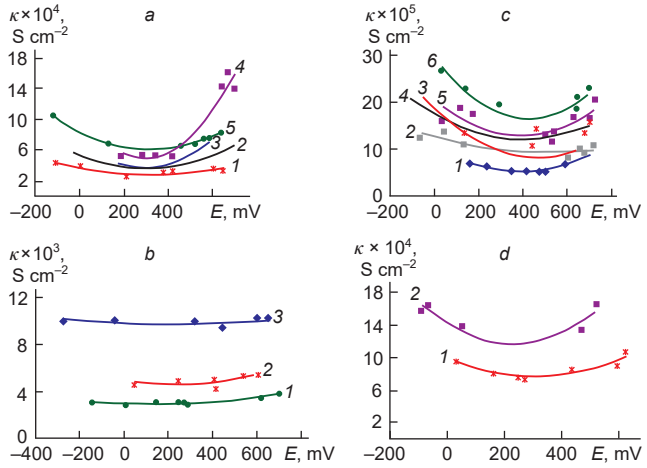

Fig. 6. Electrical conductivity as a function of potential (*vs.* normal hydrogen electrode) for CH900 (*a*, *b*) and SAIT (*c*, *d*).[78] KCl concentration, mol L^{-1}:

Curve	*1*	*2*	*3*	*4*	*5*	6
Fig. *a*	0.002	0.003	0.004	0.005	0.006	
Fig. *b*	0.05	0.1	0.2			
Fig. *c*	0.001	0.002	0.003	0.004	0.005	0.006
Fig. *d*	0.05	0.1				

measuring the surface conductivity proposed by Volfkovich *et al.*[78] is a new approach for studying EDL in porous electrodes.

Owing to the presence of various SGs, activated carbon exhibits both anion and cation exchange properties. While using electrodes based on AC materials in electrochemical devices (in particular, in CDI), it is important to know both their anion and cation exchange capacities. In a study of Volfkovich *et al.*,[83] these values for Norit and CH900 AC materials were determined to be as follows (mol g^{-1}):

Capacity	Anion exchange	Cation exchange
CH900	70	0.06
Norit	0.20	0.56

Thus, the electrochemical measurements for AC revealed the presence of a porous structure with a very broad range of linear pore dimensions and sorption, hydrophilic — hydrophobic, and ion exchange properties. It comes as no surprise that AC-based materials are widely used in various fields, particularly, in electrochemical supercapacitors and in the capacitive deionization (desalination) of water.

3. Electrochemical supercapacitors

Activated carbon is used most often in electrochemical supercapacitors.[86–93] According to the commonly accepted definition, which was first proposed by Conway, ECSCs are electrochemical devices in which quasi-reversible electrochemical charge — discharge processes take place and the galvanostatic charge — discharge curves of which are nearly linear, *i.e.*, they are similar in shape to the corresponding plots for common electrostatic capacitors.[86] The electrodes used in electrochemical supercapacitors are based on highly dispersed carbon materials with a large specific surface area. The main advantages of ECSCs over batteries are as follows:

— higher power characteristics and cyclability, which is comparable with the cyclability of traditional capacitors (up to hundreds of thousands or a million of cycles);

— efficient operation under unusual conditions (at temperatures from –50 to 60 °C) and small size;

— very high energy efficiency (the ratio of the discharge to charge energy) of some ECSCs makes it possible to use them for energy accumulation, storage, and supply and to smooth out the peak loads of electric networks;

— wide range of charge and discharge times (from fractions of a second to several hours);

— environmental safety: the disposal of many types of batteries (lead, alkaline, or lithium batteries) is associated with the release of toxic elements such as lead, nickel, lithium, fluorine, sulfur, *etc.*; conversely, ECSCs with carbon electrodes and aqueous electrolytes are nearly environmentally benign.

A drawback of ECSCs is more pronounced decrease in the voltage and stored energy density upon self-discharge compared to that of batteries.[88] This drawback could be mitigated by manufacturing high-purity ECSCs, since the self-discharge is induced by impurities in the electrolyte and electrodes.

Electrochemical supercapacitors are used most widely in road and rail transport and in various electronic devices. Depending on their function, ECSCs are classified into power, or pulse devices (those with high power density) and energy devices (those with high energy density). Depending on the design and processes that take place in ECSCs, they are classified into double layer capacitors (DLCs), pseudocapacitors (PsCs), and hybrid supercapacitors (HSCs).[86,87]

3.1. Main properties of double-layer capacitors

The functioning of DLCs is based on charging of an electric double layer of AC electrodes. The DLC design includes two highly dispersed porous polarizable electrodes and a porous separator. The energy conservation is accomplished *via* charge separation at the two electrodes with a considerable potential drop between them. These devices effectively operate under non-standard conditions, since their functioning is not limited by the kinetics of electrochemical processes, but obeys the laws of electrophysics. The DLC energy efficiency may approach 100%, because DLCs, unlike batteries, are not subject to energy losses caused by polarization of electrode reactions. The electrical charge of DLCs is determined by the EDL capacity.

The electrochemical process in DLCs can be represented as follows:

negative electrode

$$E_s + Cat^+ + e^- \rightleftharpoons E^-_s/Cat^+ \quad (4)$$

positive electrode

$$E_s + An^- \rightleftharpoons E^+_s/An^- + e^- \quad (5)$$

overall reaction

$$E_s + E_s + Cat^+ + An^- \rightleftharpoons E^-_s/Cat^+ + E^+_s/An^- \quad (6)$$

where E_S is the electrode surface, / is EDL, An^- are anions, and Cat^+ are cations.

During charging, electrons are transported from the positive electrode to the negative one through an external current source. The electrolyte ions migrate towards the electrodes. During the discharge, the electrons and ions move in the opposite directions. The charging and discharging processes are accompanied by a change in the charge at the interface. The theoretical views on the EDL capacity are based on the known Helmholtz, Stern, Gouy–Chapman, and Graham theories.[84]

Detailed electrochemical analysis of processes in ECSCs is carried out by measuring the current (I) — voltage (CV) curves at a specified linear voltage (potential) sweep rate by cyclic voltammetry (Fig. 7).

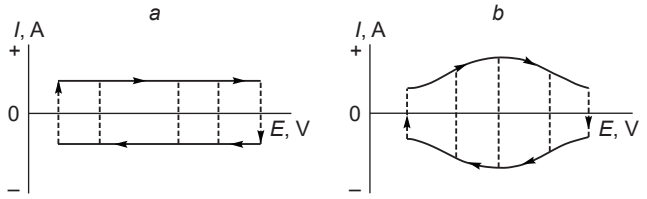

Fig. 7. Schematic views of CV curves for ideal DLC (*a*) and for PsC (*b*). The difference between the shapes of CV curves is due to the fact that the total capacitance of DLC is determined only by EDL capacitance, while in the case of PsC, it is determined by EDL capacitance and the pseudocapacitance of electrochemical reactions. The vertical dashed lines indicate the possibility of charging to intermediate potentials.[87]

Like for all ideal capacitors, the electrical capacitance of DLC (C) is inversely proportional to plate thickness (l)

$$C = \frac{э}{4\pi l} \quad (7)$$

where э is the dielectric constant of the electrolyte.

In conventional capacitors, a sheet of paper placed between the electrodes serves as the plate. These capacitors have a low specific capacitance, as the paper thickness is relatively large: several tens of micrometres. In DLC, the plate is EDL, which is a few tenths of nanometre thick; therefore, the specific capacitance per unit area of the interface between the electrode and the liquid electrolyte (C_S) is many orders of magnitude greater than that of paper capacitors. For aqueous electrolytes, C_S is in the range from 10 to 20 mF cm^{-2}, while for non-aqueous electrolytes it is a few units.[84] Lower C_S values for organic electrolytes compared to aqueous electrolytes are due to the fact that a considerable part of the surface of many carbon materials belongs to micropores into which the organic ions and molecules cannot penetrate because of their large size.[86,87]

The specific capacitance per unit electrode weight (C_g) is defined by the product

$$C_g = C_s \cdot S \quad (8)$$

Here, the specific surface area S is expressed in cm^2 g^{-1}. In order to obtain a high capacitance, electrodes with S from ~500 to 2500 m^2 g^{-1} are used in DLCs. Highly dispersed materials such as activated carbon, aerogels, carbon nanotubes and nanofibres, graphenes, carbon blacks, *etc.*, are used as the basis for these electrodes.

3.2. Influence of redox reactions of surface groups on the energy efficiency of electrochemical supercapacitors

Volfkovich and co-workers[89,90] demonstrated the influence of redox reactions of the surface groups of AC electrodes on the energy efficiency of ECSCs. The authors[89] developed a mathematical model that took into account the EDL charging and the pseudocapacitance of the SG redox reactions. It is important that the energy efficiency of ECSCs, unlike the efficiency of batteries, is not limited by the polarization of electrode reactions, but is limited only by ohmic energy losses. Therefore, the efficiency of double layer supercapacitors can approach 100%.

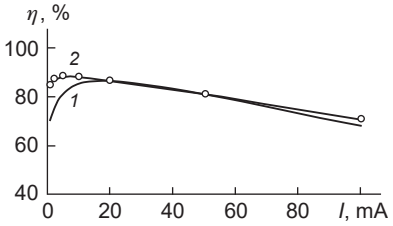

Fig. 8. Calculated (*1*) and experimental (*2*) dependences of the energy efficiency on the current for ECSCs based on the Norit activated carbon.[89]

Volfkovich *et al.*[89] calculated the energy efficiency for ECSC with electrodes based on Norit activated carbon from the experimental galvanostatic dependences of voltage on the charging and discharging time. The experimental and calculated dependences of the energy efficiency (η) on the current for symmetrical ECSCs (with two identical electrodes) are shown in Fig. 8. It can be seen that on moving to higher currents, the efficiency first increases to reach a maximum of ~90% and then decreases.

This bell-like shape of the curves can be explained as follows. At low currents, a considerable contribution to the total capacitance is made by the pseudocapacitance (battery) process characterized by low efficiency due to polarization of electrode reactions. When the current is high, the ohmic losses are involved. At intermediate currents, only EDL charging takes place, while the pseudocapacitance and ohmic losses are virtually absent. Since charging of EDL is reversible, its efficiency is maximized. This dependence of the efficiency on the current is significant when ECSCs are applied to smooth out peak loads of electric networks, because it demonstrates that in this case, it is necessary to operate in the region of maximum efficiency. The similarity of the calculated and experimental dependences of the efficiency on the current (see Fig. 8) is a piece of evidence for the accepted mechanism of ECSC operation.

As the current density decreases, the capacitance increases (Fig. 9). At high currents, this increase is relatively slow, because it is associated with a decrease in the ohmic losses. However, at low currents, there is a sharp increase in the capacitance during the charging and discharging processes, because of the significant contribution of the pseudocapacitance of the redox reactions of surface groups.

The effect of these reactions on the energy efficiency was also studied[90] for KJEC 600/Li type supercapacitor with non-aqueous electrolytes. The porosimetry curves in octane and in water for the KJEC 600 carbon black, which is similar to AC, measured by SCP method are depicted in Fig. 10. It can be seen that the porosity in octane is much higher than that in water; this attests to the presence of both hydrophilic and hydrophobic pores. It is noteworthy that these curves intersect in the region of small pores with $r^* \approx 10$ nm, that is, the curve for water is shifted towards smaller r^*. In view of the fact that octane almost perfectly wets all materials (for octane, $\theta \approx 0$), this intersection implies better wetting of the KJEC 600 carbon black with water

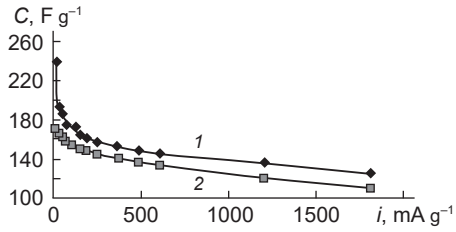

Fig. 9. Charging (*1*) and discharging (*2*) capacitance *vs.* current density for ECSC with RIKON electrodes.[89]

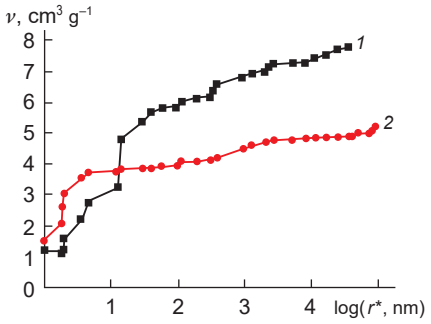

Fig. 10. Integral effective radius distribution of pores measured by the SCP method for the KJEC 600 carbon black in octane (*1*) and water (*2*).[90]

than with octane. This phenomenon, which is called superhydrophilicity, can be attributed to the presence of a large number of SGs that are hydrated in water, inducing swelling of the material. The specific surface areas calculated from the porosimetric curves were 2500 $m^2\ g^{-1}$ for octane and 2600 $m^2\ g^{-1}$ for water.

The charge and discharge curves for the KJEC 600/Li type supercapacitor at various specific currents and the dependence of the energy efficiency on the discharge current derived from these curves are presented in Figs 11 and 12, respectively. The latter plot has a maximum, like the curves in Fig. 8, and for the same reason.

Bograchev *et al.*[90] developed a mathematical model that took into account both the charging of EDL and redox reactions of SGs. A comparison of the theoretical and experimental charge — discharge curves shown in Fig. 11 indicates that they are in satisfactory agreement with each other, thus confirming the correctness of the model.

Thus, the above examples provide the conclusion that the presence of a certain type of surface groups may decrease the energy efficiency of ECSCs.

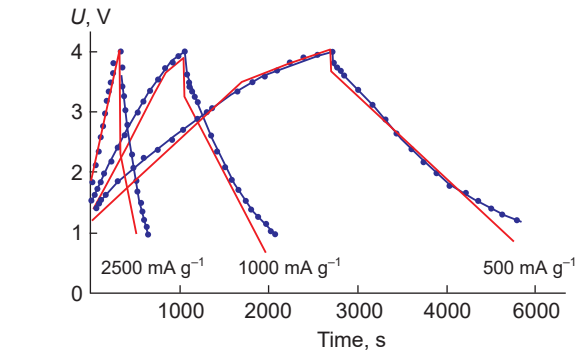

Fig. 11. Calculated (red lines) and experimental (dots) galvanostatic charge (ascending) and discharge (descending) curves for KJEC 600/Li type ECSC at specific currents of 500, 1000, and 2500 mA g^{-1}; *U* is voltage.[90]

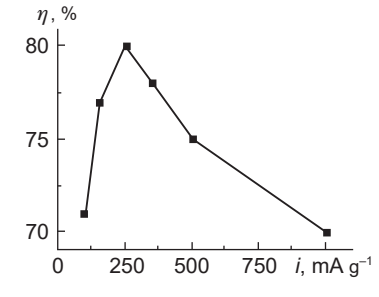

Fig. 12. Energy efficiency *vs.* specific discharge current for KJEC 600/Li type ECSC.[90]

3.3. Redox capacitors based on organic monomers. Influence of surface groups

An interesting issue is the development of pseudocapacitors containing redox pairs based on organic monomers bound to the carbon base of the electrodes by covalent bonds. As a typical example of redox capacitor, we will consider asymmetric PsC in which the positive electrode is modified with 1,2-dihydroxybenzene (C-DHB), while the negative electrode is modified with anthraquinone (C-AQ).[87] The modified carbon fabric Spectracarb 2225 was chosen as the base of the manufacture of electrodes. The specific capacitance of the DHB-modified carbon fabric electrode was 201 F g^{-1}, while that of the non-modified electrode was 141 F g^{-1}. 4-Aminocatechol used as the precursor can bind to the carbon fabric in two ways: by forming the C–C bond (structure **1**) and C–N bond (structure **2**); therefore, CV curves for DHB exhibit two peaks.[87]

Structures 1, 2

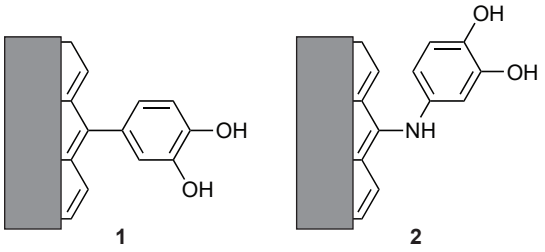

1 **2**

The C-AQ negative electrode also showed a substantial increase in the capacitance (up to 367 F g^{-1}) compared with the unmodified electrode made of AC fabric. The energy density (W) and power density (P) obtained for two ECSCs, one with unmodified (C/C type capacitor) and one with modified electrodes (C-AQ/C-DHB type PsC), are given in Table 1. It can be seen that PsC with modified electrodes provides a much higher energy density than the capacitor with unmodified carbon electrodes.

Table 1 Energy density and power density at various currents for a capacitor with unmodified electrodes (C/C type) and PsC with modified electrodes (C-AQ/C-DHB type).[87]

Current, A	C/C type capacitor		C-AQ/C-DHB type PsC	
	W, W h kg^{-1}	P, kW kg^{-1}	W, W h kg^{-1}	P, kW kg^{-1}
0.01	5.2	0.16	10.0	0.18
0.1	4.2	1.5	8.3	1.7
0.2	3.5	2.9	7.0	3.0
0.5	2.1	6.2	3.9	5.4
1.0	0.8	8.8	1.1	6.3

Activated carbons were also modified by 2-nitro-1-naphthol to manufacture ECSC electrodes that make use of the EDL capacitance and the pseudocapacitance of redox reactions of organic compounds such as *o*-aminonaphthol and *o*-naphthoquinonimine (Scheme 1).[87]

Scheme 1

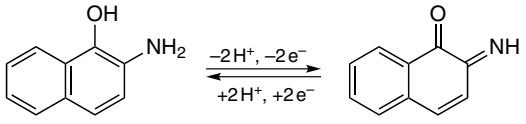

Modification of an AC electrode resulted in a specific charge of 35 mA h g^{-1}. Combination of this electrode with proton transfer agents such as Mo_2N or WO_3 results in an increase in the potential drop between the electrodes and in the corresponding increase in the specific charge, which may be used to develop HSC.

3.4. Lithium cation exchange capacitors

Original PsCs in which exchange of lithium cations between the anode and cathode takes place have been developed.[94] The action mechanism of these devices is similar to that of lithium ion batteries (LIBs). The differences between them are as follows. The operation of LIBs is based on the Faradaic reactions in the bulk of the active material. This mechanism provides an energy density (180 W h kg^{-1}) higher than that of ECSCs. However, in this case, lithium should migrate from the inner part of a cathode active particle to the surface of an anode active particle during charging, while during the discharge lithium migrates back. Thus, intercalation — deintercalation processes take place in the electrodes; owing to the very low rate of solid-phase diffusion, these processes are kinetically limited. As a result, LIBs have a very low power density (100–1000 W kg^{-1}), and recharging requires a lot of time.

In the modern lithium ion capacitors, both electrodes are based on graphene with a large specific surface area. Graphene materials with particular SGs contact with the electrolyte; this is accompanied by fast and direct adsorption of lithium and/or surface reaction of SGs (Scheme 2). This eliminates the necessity of intercalation.[87,94]

Scheme 2

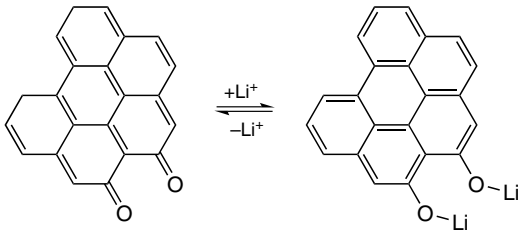

or

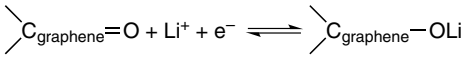

Thus, these PsCs are redox capacitors in which the energy density (160 W h kg^{-1}) and power density (100 kW kg^{-1}) are 30 and 10 times higher, respectively, than those in DLC; the power density of these devices exceeds this characteristic of LIBs by a factor of 100. Whereas in the case of conventional LIBs, several hours are required for lithium intercalation — deintercalation to be completed in both electrodes, in the case of lithium ion PsC, the time of ion migration is approximately several minutes.

However, the benefits of this mechanism decrease due to the absence of a source of lithium ions in the device; therefore, preliminary charging is required by carbon electrode lithiation in an additional cell and transfer to the supercapacitor cell in a dry box. The methods proposed to solve this problem have drawbacks. A procedure based on the use of a lithiated organic material, dilithium salt of 3,4-dihydroxybenzonitrile, has been developed.[95] This compound is capable of supplying lithium cations into a graphite electrode in the initial stage of charging. The attained energy densities are 40–60 W h kg^{-1}, the power densities are 2 kW kg^{-1}, and the cyclability reaches 15000.

Li *et al.*[96] considered several types of prelithiation of the negative electrode: short-circuit method, electrochemical method, extraction of lithium from lithiated transition metal

oxides in the positive electrode; and introduction of a lithium salt into the electrolyte.

3.5. Self-discharge of electrochemical supercapacitors with activated carbon-based electrodes

The demand for ECSCs in various fields of economy stimulates the studies and the increase in the industrial production of these devices.[86,87] The advantages of ECSCs over batteries have been noted above, together with their significant drawback–fast self-discharge, which is manifested as a voltage drop after charging and opening of the external circuit. In most publications devoted to ECSCs, self-discharge is usually neglected. Therefore, it is very important to comprehensively study this phenomenon. Kurzweil and Shamonin[97] showed that the self-discharge for two weeks is accompanied by the loss of 5 to 60% of voltage, and the rate of this process depends on the initial voltage, temperature, and the duration of charging. There are publications[88,97–124] that describe methods for measuring the self-discharge rate and propose ways to decrease it. It is clear that elaboration of measures reducing the self-discharge rate would be favourable for expanding the scope of applications of supercapacitors in various fields of national economy, in particular in arms industry.

Investigations of the self-discharge of ECSCs with electrodes based on CH900 and with an 1 M aqueous solution of $MgSO_4$ as the electrolyte have been reported by Volfkovich *et al*.[88,122] The elemental compositions of the positive and negative electrodes became sharply different after electrochemical treatment up to 1.6 V. Very high concentrations of hydrogen and oxygen caused by the formation of SGs appeared on the positive electrode. It was shown that ~70 min after the beginning of self-discharge, the logarithm of self-discharge rate is proportional to the charging voltage, while after 2000 min, the curves reach a minimum caused by the action of two opposing factors. First, a significant contribution to the capacitance is made by the pseudocapacitance of the Faradaic redox reactions of SGs and, second, the mere presence of these groups leads to increasing self-discharge rate. The former factor predominates in the low voltage region, while the latter factor prevails at ta high voltage.

3.6. Influence of surface groups of a definite composition on characteristics of electrochemical supercapacitors

In recent years, numerous original studies describing the influence of SGs on the characteristics of ECSCs have been published (see, for example, Refs 125–128). The methods used to detect SGs include IR, X-ray photoelectron, and Raman spectroscopy. The influence of SGs on the characteristics of the fibrous solid-state ECSCs used for energy storage in wearable soft electronics was studied by Hsiao and Lin.[125] Carbon fibres were treated with acid mixtures containing various ratios of HNO_3 and H_2SO_4. The highest energy density was 16.57 mW h cm^{-2} and the power density was 62.50 mW cm^{-2}. Lee and An[127] fabricated the first flexible fibrous supercapacitor with electrodes based on AC fibre with surface groups and a gel polymer electrolyte containing a redox additive to be used as a wearable energy storage device. This device showed a very high electrochemical characteristics, namely, specific capacitances of 891 and 399 mF cm^{-2} for current densities of 70.0 and 400 mA cm^{-2}, respectively.

Quite recently, a new family of two-dimensional inorganic materials called MXenes have been reported. These materials consist of atomically thin layers of transition metals carbides, carbonitrides, or nitrides. MXenes have become in high demand for the manufacture of energy storage devices, as they possess a number of remarkable properties caused by both their unique structure and adjustable SGs. MXenes are especially suitable as electrode materials for ECSCs, because they are mechanically more flexible, have a higher energy density, and have good electrochemical characteristics as compared with other materials. A review by Wang *et al*.[128] summarizes the achievements in the synthesis of MXenes and the results of studying the fundamental properties of composite materials based on them, with attention being focused on the most recent electrochemical characteristics of electrodes in electrochemical devices.

It was noted above that highly dispersed carbon materials contain a lot of diverse SGs, which considerably affect the ECSC characteristics.[129–133] The presence of SGs can change the key properties of carbon materials: wettability, conductivity, and pore size distribution; SGs can also participate in redox reactions. Most often, carbon materials contain oxygenated SGs. He *et al*.[129] reported a systematic analysis of the mechanisms of increase in the capacitance, which take into account the presence of oxygenated SGs, and the consequent mechanisms of appearance of the pseudocapacitance in acid and alkaline aqueous electrolytes.

Li *et al*.[130] modified oxygenated SGs on commercial AC by oxidation with ammonium persulfate $(NH_4)_2S_2O_8$ followed by annealing at various temperatures. The effect of surface modification on the electrochemical characteristics of ECSC electrodes was studied by X-ray photoelectron spectroscopy and Fourier transform IR spectroscopy, argon adsorption, and electrochemical testing. According to the results, the presence of oxygenated (especially carboxyl and carbonyl) SGs leads to better wettability of the pore surface, higher rate of electrolyte diffusion, and higher specific capacitance due to the additional pseudocapacitance arising in the aqueous electrolyte (6 M aqueous KOH). An excess content of oxygen resulted in blocking of some of the pores, which deteriorated the electrochemical performance; however, after annealing at 300 °C under inert atmosphere, the specific capacitance increased and the kinetic characteristics were improved. However, in an organic electrolyte (1 M Et_4NBF_4/propylene carbonate), modification of SGs *via* the oxidation with ammonium persulfate resulted in a decrease in the specific capacitance, which efficiently increased after annealing at 700 °C. Activated carbon with a hierarchical pore structure and optimized porosity is a promising material for the use in ECSCs. However, selective regulation of SGs is a difficult task. Xu *et al*.[131] used carbonization of linoleic acid under autogenic pressure at elevated temperature followed by activation with KOH to obtain carbon microspheres with a hierarchical pore structure enriched with carbonyl and carboxyl groups. Numerous micro- and mesoporous channels appeared after activation with potassium hydroxide, with the specific surface area varying from 1992 to 2414 m^2 g^{-1}. When this carbon material was used as the electrode and KOH served as the electrolyte, the capacitance of ECSCs was 365 F g^{-1} at a current density of 0.5 A g^{-1}. The two-dimensional porous carbon material prepared by Wang *et al*.[132] from pomelo peels had a large specific surface area (1927 m^2 g^{-1}) and was rich in oxygenated SGs. Therefore, when used as an ECSC electrode, it provided high capacitance (398 F g^{-1} at a current density of 1 A g^{-1}) in aqueous electrolytes and high energy density (21 W h kg^{-1}) in ionic liquids.

While studying the relationship between the oxygen-containing SGs of graphene and stability of ECSC operation, Lin *et al.*[133] synthesized reduced graphene oxide (rGO) bearing various oxygen-cobtaining groups. Hydrazine was used as the reducing agent; the reduction time was varied. According to the results of transmission electron microscopy, Raman spectroscopy, X-ray photoelectron spectroscopy, and X-ray diffraction analysis, the sp^2-bonded structure was reduced with increasing time of synthesis, and the resulting rGO had a good crystallinity because of the removal of oxygen-containing SGs. High capacitance characteristics of rGO indicate that these SGs contribute to the pseudocapacitance, and this results in a higher specific electrical capacitance. Apart from oxygen-containing SGs, nitrogen-containing groups have a pronounced influence on the ECSC characteristics.[134–138] Ilnicka *et al.*[134] investigated nitrogen-doped porous carbons for ECSC electrodes obtained from chitosan, gelatine, and green algae. The authors addressed the influence of three factors, namely, the specific surface area, the presence of SGs, and the pore structure on the electrochemical performance. Changes in the nitrogen content (from 5.46 to 10.08 mass%) and S values (from 532 to 1095 $m^2\ g^{-1}$) were attained by modifying the carbon precursor and varying the carbonization temperature. The carbons obtained in this way had a high capacitance (231 $F\ g^{-1}$ for a current density of 0.1 $A\ g^{-1}$) and cycling stability in 0.2 M K_2SO_4. Analysis of electrochemical behaviour revealed the influence of nitrogen-containing SGs on the pseudocapacitance. Groups containing quaternary and pyrrole nitrogen induced an increase in the pseudocapacitance owing to the presence of positive charge; therefore, they facilitated the electron transfer at high current loads; graphite/quaternary nitrogen structures were found to be most important and to influence energy storage characteristics.

A high-performance foldable solid-state asymmetric ECSC was developed using one-step scalable chemical oxidation and MXene ink painting of nitrogen-doped carbon fibre textile substrate.[135] The used O- and N-functionalized carbon fibre and MXene materials with opposite potentials combine the electrochemical behaviours of highly dispersed pseudocapacitance carbon materials, particularly, high charging and discharging rate and great pseudocapacitance. By varying the oxidation time and the MXene loading, an expanded potential window (1.6 V) and high energy density (277.3 mW h cm^{-2}) were attained for the active layers of MXene-decorated ECSC electrodes.

In recent years, porous carbon electrode materials obtained from biopolymers such as chitin and chitosan (structures **3** and **4**, respectively) have attracted attention owing to their ready availability, high porosity, low specific weight, natural biodegradability, and environmental friendliness. The structure of these compounds comprises a long linear chain, which can be functionalized with oxygen- and nitrogen-containing groups *via* β-glucosidic linkage. They can be used as templates to design electrode materials with tunable and clearly defined geometry. The application of chitin- and chitosan-based materials as ECSC electrodes was discussed by Vinodh *et al.*[136]

Structures 3, 4

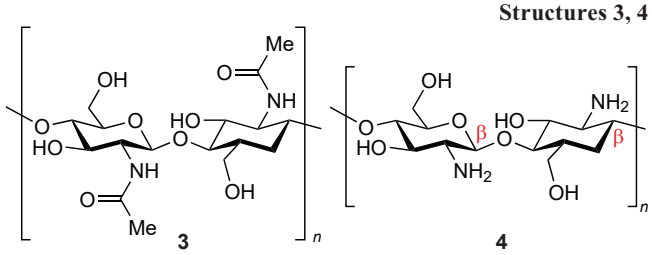

Low energy density is a key problem hampering commercialization of Zn ion hybrid supercapacitors. This problem is due to the lack of high-capacitance cathode materials, especially for high current density. Wang *et al.*[137] used biomass to synthesize carbon nanosheets with a porous hierarchical structure functionalized with oxygen-containing groups containing some nitrogen. The materials thus obtained, which were used as cathodes, possessed a high capacitance, particularly, 220.1 mA h g^{-1} at a current density of 0.2 $A\ g^{-1}$ and 118.2 mA h g^{-1} as the current density increased 100-fold (up to 20 $A\ g^{-1}$). Zinc-ion hybrid supercapacitors with these cathodes demonstrated an ultrahigh energy density (181.6 W h kg^{-1}). Experimental results and theoretical calculations showed that the hierarchical pore structure of ultrathin nanosheets with macro-, meso-, and micropores is favourable for enhancing the physical adsorption of Zn^{2+} cations, while the introduction of surface pyrrole and carboxyl groups synergistically increases the chemical adsorption of Zn^{2+} cations.

Liu *et al.*[138] used waste polyimide (PI) film to manufacture several flaky porous carbon materials to be used ECSC electrodes. The structures of pores and SGs of the porous carbon materials were optimized by activation with potassium hydroxide. The relationship between the pore structure, carbon matrix, surface groups, and electrochemical performance was studied using nitrogen adsorption, X-ray diffraction techniques, Raman spectroscopy, X-ray photoelectron spectroscopy, Fourier transform IR spectroscopy, and electrochemical measurements. The flaky porous carbon had a calibrated size distribution of hierarchical pores and were rich in oxygen- and nitrogen-containing SGs. Electrodes made of these materials possessed high specific capacitance (482 $F\ g^{-1}$), being superior in this characteristic to the electrodes made of porous carbons based on PI film obtained by physical activation and also to AC-based commercial electrodes.

MXenes are widely used for microsupercapacitors. Among them, the most studied systems are $Ti_3C_2T_x$, where T are functional SGs, for example, F, OH, and O. These MXenes are obtained by etching the A layer of the initial Ti_3AlC_2 MAX phase. Functional groups play an important role in the charge accumulation and they should be controlled in order to improve the electrochemical performance of MXenes. Peng *et al.*[139] used bacterial cellulose (BC) with a definite content of SGs to increase the distance between MXene layers to allow more ions to be adsorbed on the surface. Then a solution of KOH was added to treat the mixed solution of MXene and BC. A Fourier transform IR spectroscopic examination confirmed that the surface of the MXene/BC film bore a large number of SGs. According to X-ray photoelectron spectroscopy data, the strength of oxygen SGs on the treated film surface was greater than that for the untreated film. Electrochemical performance testing demonstrated that the composite film treated with a KOH solution, being used as a microsupercapacitor electrode, had a specific capacitance of 223 mF cm^{-2} and an energy density of 42 mW h cm^{-2}; these values were better than those of the composite film electrode without KOH treatment (specific capacitance of 161 mF cm^{-2} and energy density of 31 mW h cm^{-2}).

A series of studies [140–142] addresses carbons bearing nitrogen-containing SGs. *p*-Nitroaniline was used as a universal precursor for the selective preparation of porous carbons with a large content of nitrogen SGs. Owing to the catalytic effect of pyridine and pyrrole N-sites and to high specific surface area and conductivity values, the optimized porous carbon is favourable for redox reactions. ECSCs fabricated using this material

showed a very high specific capacitance (1783 F g^{-1} at a current density of 1 A g^{-1}), high rate capability (800 F g^{-1} at a current density of 6 A g^{-1}), and an excellent cycling stability.

Currently, original nanostructures are often manufactured using biomass as the source of carbon. However, the biological diversity does not favour the use of biomass for high-precision applications. Lian *et al.*[141] obtained porous carbon without resorting to the known pore generation methods (such as alkaline activation). The authors used biomass that was subjected to biodegradation. From the obtained carbon-containing components of the biomass, nanospheres (NC) and nanosheets were synthesized. These nanostructures were modified with *p*-phenylenediamine (PPD). The nanospheres modified with functional groups (NC-PPD) were tested as electrodes for flexible ECSCs and CDI units. The following results were obtained: the NC-PPD//NC-PPD assembly in ECSC provided a high energy density of 8.8 W h kg^{-1}, with the highest power density being 2.5 kW kg^{-1}. The salt capacity for the CDI unit can be as high as 33.2 mg g^{-1}.

Magnetic nanoparticles with a high surface area to volume ratio are present in materials meant for various purposes, including tunable optical, electrical (particularly, for ECSCs), catalytic, biological, and nanofluid materials. However, to attain desired material properties, it is strictly necessary to appropriately functionalize the nanoparticle surface. Singh *et al.*[142] used aryldiazonium salts to modify $NiFe_2O_4$ nanoparticles. As a result, stable SGs were formed on nanoparticles functionalized with organic molecules. The modified nanoparticles exhibited a sharp increase in the specific capacitance in 3 M KOH (~1279 F g^{-1}) compared with unmodified $NiFe_2O_4$ particles.

Carbon materials with SGs consisting of either a small or a large number of chemical elements can be used as electrodes in ECSCs. In order to markedly improve the electrochemical performance of ECSCs, Zheng *et al.*[143] obtained carbon materials doped with heteroatoms (N, P, S, O) to be used as electrodes. Heteroatom doping leads to higher pseudocapacitance and electrical conductivity, better wettability, higher capability of reversible ion accumulation, and increasing rate of electrochemical processes. Structural nitrogen atoms include pyridine, pyrrole, quaternary (graphite) nitrogen, and pyridine N-oxide. The pyrrole and pyridine nitrogen atoms increase the pseudocapacitance. Nitrogen accelerates the transfer of electrons. Phosphorus atoms can bind to oxygen atoms to form a single bond. Sulfur is often present near the edge or at defective sites of carbon hexagons, being a part of thiophene or SO_x oxide. Oxygen binds to carbon through single, double, or another bond in the carbon skeleton. Zheng *et al.*[143] described the mechanism of heteroatom doping of carbon materials and its influence on the characteristics of the obtained doped materials, which are used as electrodes for ECSCs.

Study of efficient and durable electrode materials is a crucial factr for the design of high-performance HSCs. Chen *et al.*[144] deposited Fe_3O_4/Fe nanoparticles modified with phosphate ions (P–Fe_3O_4/Fe) on carbon nanosheets (CNS) by a two-step calcination with sodium sulfate in the solid state. Owing to the synergistic effect of the components and unique two-dimensional architecture, the prepared P–Fe_3O_4/Fe/CNS electrode provided high energy storage characteristics with a high specific capacitance of 427.4 F g^{-1} at a current density of 1 A g^{-1}. Then, phosphate-functionalized P–Co_9S_8/CoS nanoparticles attached to carbon nanosheets were prepared by the same procedure; these materials provided a highest specific capacity of 544.6 C g^{-1} at the same current density of 1 A g^{-1}. The assembled P–Co_9S_8/CoS/CNS//P–Fe_3O_4/Fe/CNS hybrid supercapacitor had a high energy density of 73.4 W h kg^{-1}, with the power density being 1041.7 W kg^{-1} in an alkaline electrolyte. The authors proposed an effective structure for the design of high-performance HSCs with effective electrodes produced by phosphate functionalization using a sodium sulfate template.

4. Capacitive deionization of water

Many countries lack sufficient supplies of clean fresh water for domestic, agricultural, and industrial use.[145] According to the prediction of environmentalists, approximately 2.5 billion people would suffer from acute shortage of clean water by 2025. Purification of aqueous solutions (including desalination of seawater) is mainly performed by the following methods: electrodeionization, distillation, ion exchange, chemical treatment, freezing, reverse osmosis, and electrodialysis. In recent years, the process of capacitive deionization of water has been actively developed in advanced countries.[146–155] According to this process, in CDI cell, the liquid feed flow is pumped between two porous electrodes (*e.g.*, AC electrodes) with a large specific surface area (from ~500 to 2500 m^2 g^{-1}), with the potential difference between the electrodes being more than 1.2 V (Fig. 13).

Ions with a definite charge sign were electrostatically adsorbed on the inner surface of the oppositely charged electrode. Thus, EDL charging and solvent deionization take place. After a certain period of time, the electrode surface saturated by adsorbed ions should be regenerated. The regeneration is attained by electrode polarity reversal or by opening of the circuit. This is accompanied by ion desorption from the electrodes, and the solution flow at the outlet of the cell becomes more concentrated. A CDI unit, which consists of at least two electrochemical cells, usually operates continuously. For some period of time, one cell performs deionization, while the other cell concentrates the solution. This gives two products, that is, deionized water and a concentrated solution, which may find use in the national economy. Most often, ~80% of the feed solution enters the deionization cell, while the other 20% is supplied to the regeneration cell to concentrate the solution.

The most important benefit of CDI is the minimum energy consumption, which amounts to approximately one third of the energy consumption involved in the main competing method, reverse osmosis, which is now widely used to desalinate water.[156,157]

The advantages of CDI over other desalination techniques are as follows:

— low operation costs;
— long cycling time;
— functioning to provide different desalination levels;

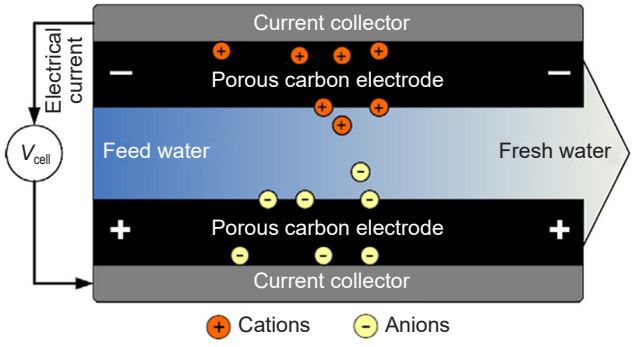

Fig. 13. Diagram of CDI cell.[151]

— low content of foreign particles in the pores (minimum clogging of pores);

— during regeneration (concentration), a considerable part of energy returns to the unit; therefore, the energy spent for deionization is partly recovered;

— in the coming years, CDI efficiency is expected to significantly increase due to the high science-intensity of this technique.

It was shown[158] that the amount of energy consumed in a CDI unit for water desalination approaches the thermodynamic minimum. A comparison of specific energy consumption for the production of 1 m^3 of desalinated water (W_{H_2O}) by a number of methods including reverse osmosis (RO), electrodialysis (Ed), multistep distillation (MD) and CDI is presented below[145] demonstrates the advantage of CDI.

Method	RO	Ed	MD	CDI
W_{H_2O}, kW h m^{-3}	2–6	0.4–8.7	10–58	0.1–2.03

Almost the only drawback of CDI is the necessity to design new high-performance units. It is clear that this problem will be overcome with time.

4.1. Process designs of the capacitive deionization of water

Apart from the basic CDI process, there are various other process designs. The membrane capacitive deionization (MCDI) is one of the most popular CDI techniques.[159–171] In this process, an anion exchange membrane is in contact with the positively charged electrode, while a cation exchange membrane is in contact with the negatively charged electrode. A separator is located between the membranes, and the separator pores are filled with the aqueous solution being pumped. The anion exchange membrane prevents cation transport towards the anode, while the cation exchange membrane suppresses almost completely the anion transport towards the cathode.

It was noted above that the lower energy consumption of CDI compared with other desalination techniques is, first of all, due to the fact that during the discharge (regeneration) stage, a certain part of the energy returns to the unit and, hence, the energy spent for charging (deionization) is partly recovered. The same is true for MCDI.[160] The time variation of the voltage during charging and discharging stages in the galvanostatic operation mode of MCDI can be followed by the data shown in Fig. 14.

One more type of CDI is flow electrode capacitive deionization (FCDI).[168–171] A dispersion of a carbon material (usually AC) in an aqueous electrolyte is used, most often, as the dispersed electrode. FCDI provides continuous deionization and good desalination characteristics. The advantages of FCDI also include the ability to deionize solutions with high salt concentrations, including seawater. Efficient operation of FCDI units with low energy consumption requires a high-capacity flow electrode with a low electrical resistance. Desalination characteristics of flow electrode cells with electrodes based on spherical AC particles and aqueous electrolytes with different NaCl contents were investigated. In an FCDI unit, the flow of the feed solution is split into two unequal parts, the greater of which is fed to the electrochemical cell to be desalinated, while the smaller one enters the electrochemical cell to be concentrated.

The next stage in the upgrading of CDI technique was the design of a unit containing both the flow electrodes and anion and cation exchange membranes. This unit for the production of pure water combines the benefits of MCDI and FCDI, *i.e.*, high degree of deionization and high production rate.[169]

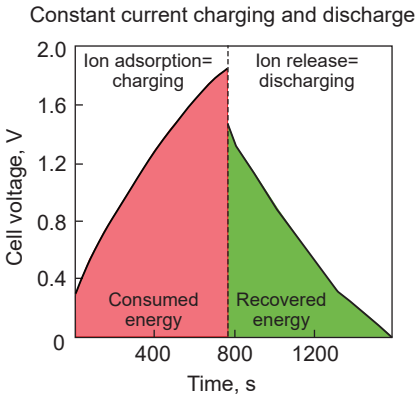

Fig. 14. Diagram of time variation of the voltage during the charging and discharging stages. The resulting energy is proportional to the difference between the areas under the charging and discharging curves.[171]

4.2. Production of pure drinking water

Drinking water is meant for the intake by living organisms and characterized by low salt content. In each country, the composition and properties of drinking water are regulated by law, and the specifications for the quality of drinking water differ from country to country (in some cases, significantly).

It was shown above that AC possesses both anion and cation exchange properties and surface conductivity in pure water (see Section 2.3); therefore, it is the electrode material of choice for CDI cells. In these units, the limiting factor is the porous separator, because water in the separator pores has a very high resistance, which results in a very high energy expenditure. Therefore, mosaic ion exchange membranes possessing both anion and cation exchange properties were devised.[83,172,173]

In mosaic membranes, the anion and cation exchange resin particles are mixed (Fig. 15). These membranes possess quite adequate ionic conductivity even in pure water; therefore, they started to be used in CDI units instead of the usual porous separators. Figure 16 shows the concentration dependences of

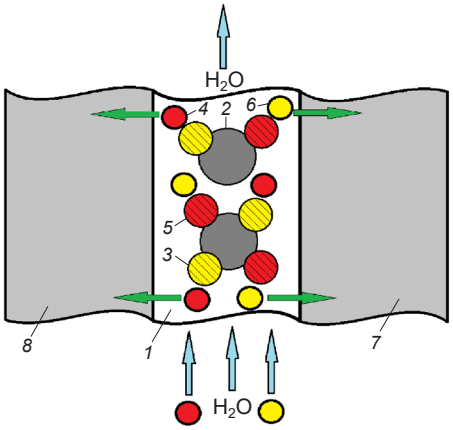

Fig. 15. Structure of the mosaic membrane. (*1*) polymer matrix; (*2*) micropores; (*3*) positively charged fixed SGs incorporated in the anion exchange resin particles; (*4*) anions; (*5*) negatively charged SGs incorporated in the cation exchange resin particles; (*6*) cations; (*7* and *8*) electrodes.[47]

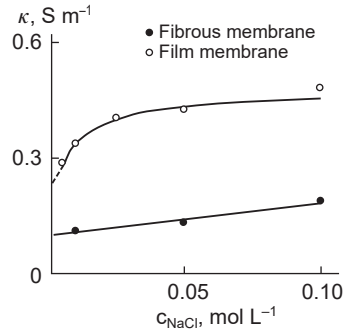

Fig. 16. Concentration dependences of the specific conductivity at very low concentrations of NaCl in solution for two types of mosaic membranes: fibrous and film membranes.[83]

the electrical conductivity at very low salt concentrations in aqueous solutions for two types of mosaic membranes, fibrous and film ones.[83] It can be seen that for both types of membranes, the specific conductivity is quite high even in pure water. This is due to the above-mentioned presence of anion and cation exchange SGs. Electrochemical measurements were carried out for static type CDI cells (without a solution flow).[83] The cell contained two AC electrodes based on the Norit carbon and a mosaic membrane located between the electrodes. The membrane and electrode pores were impregnated with pure water. The cyclic capacitance — voltage curves at different potential sweep rates (w) are presented in Fig. 17.

The following operation mechanism for an electrochemical cell with pure water was established (Fig. 18). When the electric field is switched on, the counter-cations of one AC electrode hop by the relay mechanism, owing to the surface conductivity, from one counter-cation to another and to the mosaic membrane where they migrate to the opposite electrode by a similar mechanism. At the same time, the counter-anions of the second AC electrode hop by the relay mechanism from one counter-anion to another, and then to the mosaic membrane where they are transported from one counter-anion to another, also by the relay mechanism, and then migrate to the opposite electrode in which they hop from one counter-anion to another. That is how EDL is charged. As can be seen, the shape of the cyclic capacitance — voltage curves shown in Fig. 17 *a* corresponds to the shapes of similar curves for DLC, and at the lowest potential sweep rate of 0.1 mV s^{-1}, it has a nearly rectangular shape, *i.e.*, it characterizes the EDL charging (see the upper curves in Fig. 7).

The cyclic capacitance — voltage curves for a static electrochemical cell with the Norit electrodes and a mosaic membrane for various KCl concentrations in an aqueous solution at a constant potential sweep rate of 0.1 mV s^{-1} are shown in Fig. 17 *b*. It can be seen that these double-layer curves nearly

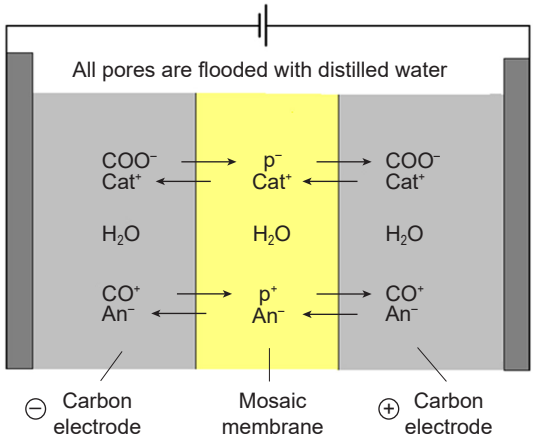

Fig. 18. Operation of a water-flooded membrane electrode assembly containing two AC electrodes and a mosaic membrane. Designations: Cat^+ are cations, and An^- are anions, p^+ are counter cations, p^- are counter anions.[83]

coincide with each other. Thus, the salt concentration has almost no effect on the capacitance of EDL of carbon electrodes, unlike that of metal electrodes such as platinum or mercury ones. It is known that the diffuse part of the capacitance increases with increasing electrolyte concentration.[84] From this it follows that the capacitance of EDL of activated carbon electrodes is determined by virtually only SG concentration.

4.3. Redox reactions of surface groups in the capacitive water deionization units

Volfkovich *et al.*[28,174,175] studied the operation of ECSCs as parts of CDI units. Electrochemical supercapacitors were impregnated with various electrolytes (aqueous solutions of salts), which were subjected to deionization. Analysis of the capacitance of ECSCs with VISKUMAK and CH900 AC electrodes as a function of the current over a broad range of currents (Fig. 19) revealed the presence of SG redox reactions.[174,175] The capacitance values were derived from the galvanostatic curves. The dependence of the integral electrochemical capacitance of the CH900 electrode on the current density in a solution of a mixture of $CaCl_2$, $NaHCO_3$, and $MgSO_4$ salts (Fig. 19 *b*) indicates that as the current decreases, the capacitance first increases, then reaches a plateau, and then sharply increases again. This pattern of dependence is due to the relatively high ohmic losses at high currents. As the current decreases, these losses decrease and the capacitance smoothly increases. When the current further decreases, the

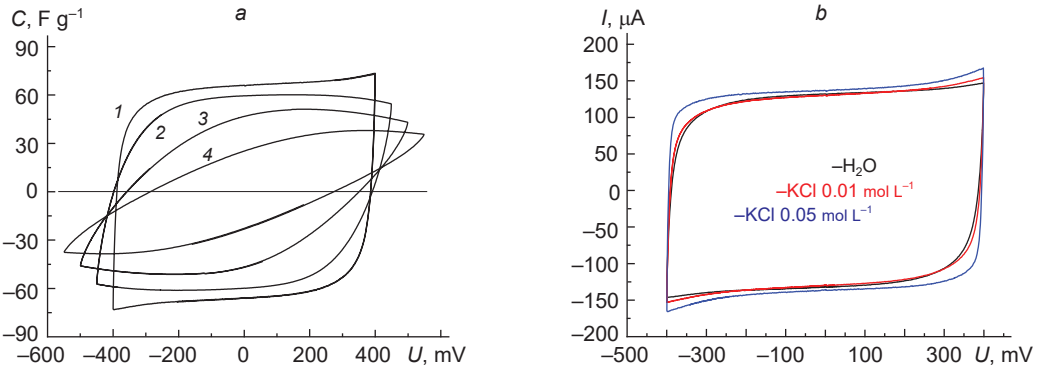

Fig. 17. Electrical capacitance (*a*) and current (*b*) *vs.* voltage measured in a CDI cell. Fig. *a*: $c_{KCl}=0$; $w=0.1$ (*1*), 0.5 (*2*), 2 (*3*), 5 mV s^{-1} (*4*); Fig. *b*: $w=0.1$ mV s^{-1} (Ref. 83).

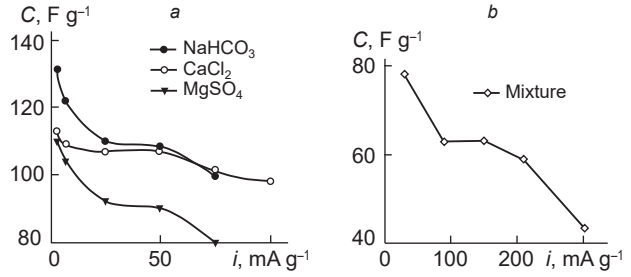

Fig. 19. Specific capacitance of the VISKUMAK activated carbon electrode *vs*. current density for $NaHCO_3$, $CaCl_2$, and $MgSO_4$ (*a*); specific capacitance of the CH900 activated carbon electrode *vs*. current density for the mixture: $CaCl_2$ (660 mg L^{-1}) + $NaHCO_3$ (373 mg L^{-1}) + $MgSO_4$ (644 mg L^{-1}) (*b*).[47]

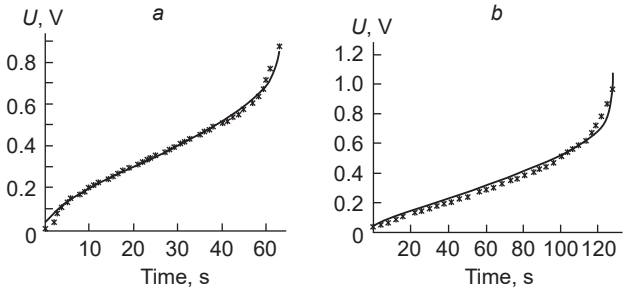

Fig. 20. Experimental (dots) and calculated (continuous lines) galvanostatic charging curves for a current density of 2.8 A cm^{-2} for SAIT AC electrodes in a $NaHCO_3$ solution (*a*) and VISKUMAK AC electrodes in a $CaCl_2$ solution (*b*).[47]

ohmic losses at the plateau of the curve are small, and the capacitance is virtually determined by the EDL charging alone; this capacitance remains approximately invariable until the pseudocapacitance of the Faradaic reactions starts to make a substantial contribution to the total capacitance. It was found[174,175] that for AC electrodes, the Faradaic reactions are mainly represented by quasi-reversible redox reactions of SGs (see Section 3.2). For a mixture of $NaHCO_3$, $CaCl_2$, and $MgSO_4$ salts, the specific capacitance of EDL was 63 F g^{-1}. The same procedure for estimating EDL capacitance was also used for solutions of other salts.

It is noteworthy that the plots of the capacitance *vs*. current for the VISKUMAK and CH900 AC electrodes also contain a characteristic plateau.

Volfkovich *et al*.[174,175] proposed a mathematical model for calculating the galvanostatic curves of ECSCs. The model uses the capacitances of EDL derived from the dependences similar to those shown in Fig. 19. Typical calculated and experimental galvanostatic voltage — time curves for charging of the SAIT and VISKUMAK AC electrodes for various currents are summarized in Fig. 20. The theoretical curves were calculated using the proposed model. It can be seen that the experimental and theoretical curves are similar, and this attests to correctness of the model, which takes into account the SG redox reactions, and validates the above method for determining the EDL capacitance.

5. Fuel cells with proton exchange membranes

A fuel cell with a proton exchange membrane is the most widely occurring and efficient device for converting the fuel chemical

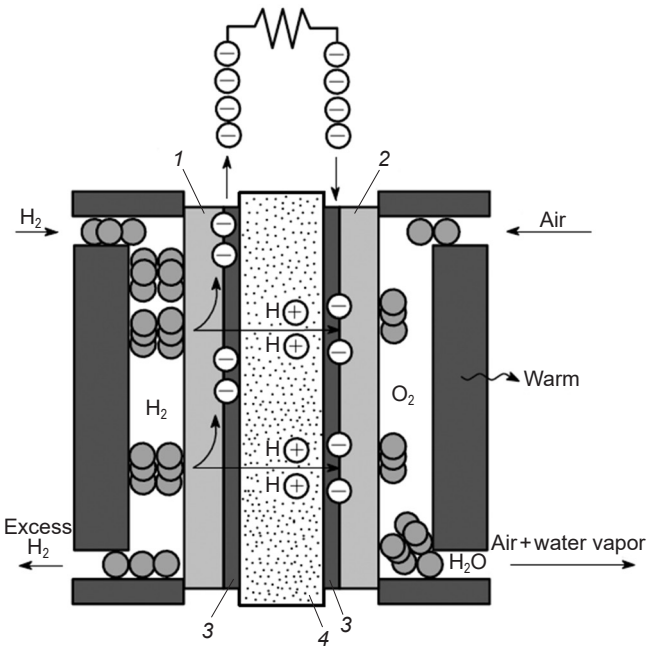

Fig. 21. Scheme of PEMFC. (*1*, *2*) Gas diffusion layers, (*3*) catalyst layer, (*4*) proton exchange membrane.[10]

energy to electricity.[87,176,177] The operation of PEMFC is provided by flows of liquid and gaseous reactants and products of electrochemical reactions in a membrane electrode assembly (MEA), which consists of the following contacting porous components: two catalyst layers, a proton exchange membrane, and two gas diffusion layers (Fig. 21).

The pore structure and hydrophilic — hydrophobic properties of MEA components substantially affect the velocity and direction of liquid and gaseous flows, and, consequently, the PEMFC operation efficiency. For better understanding of the heat and mass transfer processes in PEMFC and for their mathematical modelling and optimization, it is necessary to know the pore structure and hydrophilic — hydrophobic properties of MEA components. Water is present in PEMFC in both gaseous and liquid states. Some of the pores in MEA, mainly those formed by catalyst particles, possess hydrophilic properties and are wetted with water. Other pores in carbon particles and in some hydrophobic polymer particles, *e.g*., in polytetrafluoroethylene (PTFE) agglomerates, remain dry during fuel cell operation and, hence, they serve as transport channels for gaseous reactants and products (oxygen, hydrogen, water vapour). The efficiency of operation of such fuel cells depends on the so-called water management related to the directions of liquid and water vapour flows in MEA and in its pore system.[178–180]

The catalyst layer in PEMFC is a complex composite system, which generally contains nanosized particles of platinum catalysts supported on larger-size porous carbon (Fig. 22). The support provides the electronic conductivity of the catalyst layer. The ionomer is responsible for the proton conductivity of the catalyst layer. Liquid water is transported across the catalyst layer through the hydrophilic pores of the ionomer. The transfer of active gases (hydrogen and oxygen) to the surface of catalyst particles and the removal of the reaction products (water vapour) occur through the hydrophobic pores. An optimal volume ratio between the ionomer and the carbon support ensures sufficient ionic and electronic conductivities. The structure and

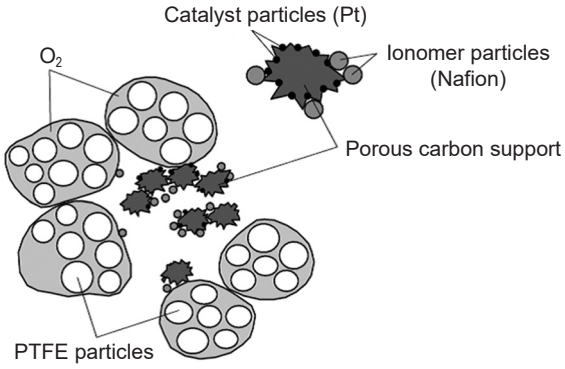

Fig. 22. Structure of the catalyst layer in PEMFC.[10]

hydrophilic — hydrophobic properties of carbon supports considerably influence the efficiency of PEMFC operation.

Volfkovich and Sosenkin,[10] who studied a catalyst layer with 40% Pt on Vulcan XC-72 carbon black and 5% ethanol solution of Nafion ionomer, used the standard contact porosimetry method. However, other types of carbon supports were not used in the experiments. The hydrophilic — hydrophobic properties and the pore structure of catalytic systems with various carbon supports and the changes in the properties of these systems after several stages of production of the catalyst layer were addressed in another publication.[181] The authors studied ten carbon supports: Anderson Ax-24 activated carbon; Vulcan XC-72 carbon black; a few Sibunit blacks; and KVU-1 and KVU-2 nanofibres. These carbon materials were studied before and after the deposition of the ionomer.

It was concluded that the degree of pore blocking by the ionomer depends on the nature and number of functional SGs. It was found that deposition of the ionomer induced hydrophobization of most carbon materials (in particular, Vulcan XC-72) and hydrophilization of other materials (*e.g.*, KVU-1). The dependences of water contact angle on the pore radius for Vulcan XC-72 and KVU-1 before and after ionomer deposition are shown in Fig. 23. It can be seen that the ionomer deposition on Vulcan XC-72 leads to hydrophobization (increase in the water contact angle) and the deposition of the KVU-1 nanofibre leads to hydrophilization.

The hydrophilic–hydrophobic properties of the carbon supports are determined by the nature and concentration of SGs, which depend on the preparation procedure of this carbon material. The schematic images of the ionomer with sulfo groups pointing to the interior and the exterior of Vulcan XC-72 and KVU-1 particles, respectively, are depicted in Fig. 24.

In the Vulcan XC-72 carbon black, the hydrophobic fluoroplastic chains $(-CF-CF_2-)_n$ are located outside, which

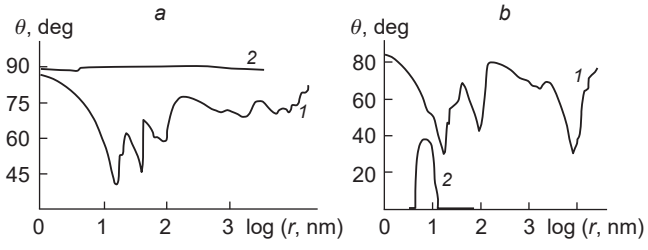

Fig. 23. Water contact angle *vs*. pore radius for the carbon supports Vulcan XC-72 (*a*) and KVU-1 (*b*) before (*1*) and after (*2*) deposition of the ionomer.[181]

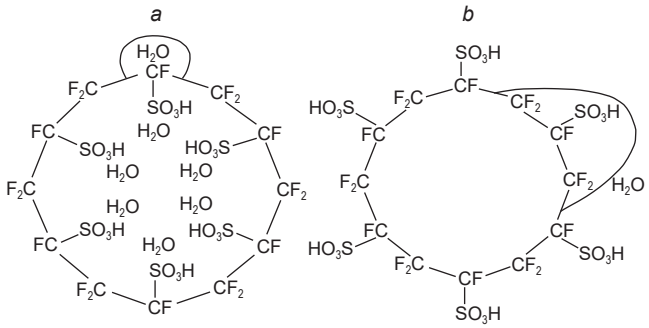

Fig. 24. Schematic image of the ionomer particle introduced into Vulcan XC-72 (*a*) and KVU-1 (*b*).[181]

results in particle hydrophobization, while in the case of KVU-1, hydrophilic sulfonic groups are outside the particles, and this leads to hydrophilization of the catalyst layer. The effect of hydrophobization of the catalyst layer by the ionomer is a non-trivial and practically important result, since the inner space of the ionomer is hydrophilic due to hydration of the sulfo groups. In this case, the ionomer acts as both a hydrophobizer for the catalyst and as a proton conductor. This is very important for optimization of the catalyst layer structure in PEMFC.¶ The inversion of sulfo groups in the outer layer of the Nafion ionomer particles depending on the type of the carbon support was first established by Volfkovich *et al*.[181]

* * *

The effect of surface groups on the properties of disperse systems is a relevant research topic, the importance of which is due to the following. Specialists in science and technology often deal with many disperse materials: activated carbons, graphenes, carbon nanotubes, carbon blacks, *etc*., which occur as parts of important devices such as electrochemical superconductors, units for the capacitive deionization of water, and fuel cells with proton exchange membranes. Most disperse objects contain numerous surface groups, which affect the operation of electrochemical devices.

Evidently, the importance of this area necessitates further studies of the topics addressed in this review, including the influence of redox reactions of the surface groups on the energy efficiency of electrochemical supercapacitors, the operation of water capacitive deionization units, redox capacitors based on organic monomers, and lithium ion capacitors, functioning of cation/anion exchange mosaic membranes, which provide the possibility of obtaining pure drinking water, and catalyst layers in fuel cells with proton exchange membranes.

This review was prepared with the financial support of the Ministry of Science and Higher Education of the Russian Federation.

6. List of abbreviations and symbols

AC — activated carbon,
CDI — capacitive deionization of water,

¶ It is of interest that, without explaining the reasons, some companies that use Vulcan XC-72 no longer add the PTFE hydrophobizer to the catalyst layer with the Nafion ionomer. Apparently, it was found empirically that in this case, the delivery of active gases (oxygen and hydrogen) to the surface of catalyst particles does not restrict the rate of electrochemical reactions.

CV — current–voltage (curve),
DLC — double-layer capacitor,
ECSC — electrochemical supercapacitor,
EDL — electric double layer,
HSC — hybrid supercapacitor,
LIB — lithium ion battery,
MEA — membrane electrode assembly,
rGO — reduced graphene oxide,
PEMFC — proton-exchange membrane fuel cell,
PsC — pseudocapacitor,
PTFE — polytetrafluorethylene,
SCP — standard contact porosimetry (method),
SG — surface group,
ZCP — zero-charge potential,
C — electric capacitance,
E — potential,
E_{stat} — stationary potential,
l — plate thickness,
I — current,
i — current density,
κ — electrical conductivity,
κ_{sg} — conductivity of the SG counter ions;
κ_{sch} — conductivity of surface groups,
κ_v — electrical conductivity of a free equilibrium solution,
r^* — effective pore radius,
r — true pore radius,
S — specific surface area,
Q — exchange capacity,
U — voltage,
W — specific energy,
v — specific pore volume,
w — potential sweep rate,
η — efficiency,
θ — water contact angle,
э — dielectric constant of the electrolyte.

7. References

1. H.Li, Y.Gao, L.Pan, Y.Zhang, Y.Chen, Z.Sun. *Water Res*., **42**, 4923 (2008); https://doi.org/10.1016/j.watres.2008.09.026
2. L.Wang, M.Wang, Z.-H.Huang, T.Cui, X.Gui, F.Kang, K.Wang, D.Wu. *J. Mater. Chem*., **21**, 18295 (2011); https://doi.org/10.1039/c1jm13105b
3. P.-I.Liu, L.Ch.Chung, Ch.-H.Ho, H.Shao, T.-M.Liang, R.-Y.Horng, M.-Ch.Chang, Ch.Chi. *J. Colloid Interface Sci*., **446**, 352 (2015); https://doi.org/10.1016/j.jcis.2014.12.007
4. H.Li, Y.Ma, R.N.Li, Y.Ma, R.Niu. *Separati. Purificat. Technol*., **171**, 93 (2016); https://doi.org/10.1016/j.seppur.2016.07.019
5. M.Shi, X.Hong, C.Liu, H.Qiang, F.Wang. *Chem. Eng. J*., **453**, 139764 (2023); https://doi.org/10.1016/j.cej.2022.139764
6. Yu.A.Chizmadzhev, V.S.Markin, M.R.Tarasevich, Yu.G.Chirkov. *Macrokinetics of Processes in Natural Media.* (*Makrokinetika Protsessov v Poristykh Sredakh)*. (Moscow: Nauka, 1971)
7. I.G.Gurevich, Yu.M.Volfkovich. V.S.Bagotskii. *Liquid Porous Electrodes.* (*Zhidkostnye Poristye Elektrody)*. (Minsk: Nauka i Tekhnika, 974)
8. H.Strathmann. *Desalination*, **264**, 268 (2010); https://doi.org/10.1016/j.desal.2010.04.069
9. V.S.Bagotskii, A.M.Skundin. *Chemical Current Sources.* (*Khimicheskie Istochniki Toka)*. (Moscow: Energoisdat, 1981)
10. Yu.M.Volfkovich, V.E.Sosenkin. *Russ. Chem. Rev*., **81**, 936 (2012); https://doi.org/10.1070/RC2012v081n10ABEH004281
11. J.G.Gamaethiralalage, K.Singh, S.Sahin. *Chem. Sci*., **12**, 10334 (2021); https://doi.org/10.1039/D1SC00915J
12. Z.Chen, X.Xu, Z.Ding, K.Wang, X.Sun, T.Lu. *Chem. Eng. J*., **407**, 127148 (2021); https://doi.org/10.1016/j.cej.2020.127148
13. F.Yang, Y.He, L.Rosentsvit, M.E.Suss, X.Zhang, T.Gao. *Water Res*., **200**, 117222 (2021); https://doi.org/10.1016/j.watres.2021.117222
14. M.E.Suss, T.F.Baumann, W.L.Bourcier, C.M.Spadaccini, K.A.Rose, J.G.Santiago, M.Stadermann. *Envirom. Sci*., **5**, 9511 (2012); https://doi.org/10.1039/c2ee21498a
15. S.Porada, R.Zhao, A.Van Der Wal, V.Presser, P.M.Biesheuvel. *Prog. Mater. Sci*., **58**, 1388 (2013); https://doi.org/10.1016/j.pmatsci.2013.03.005
16. T.Lu, Y.Liu, X.Xu, L.Pan, A.A.Alothman, J.Shapter. *Separat. Purifcat. Technol*., **256**, 117771 (2021); https://doi.org/10.1016/j.seppur.2020.117771
17. Y.Cai, Y.Wang, R.Fang, J.Wang. *Separat. Purifcat. Technol*., **280**, 119828 (2022); https://doi.org/10.1016/j.seppur.2021.119828
18. M.A.Anderson, A.L.Cudero, J.Palma. *Electrochim. Acta*, **55**, 3845 (2010); https://doi.org/10.1016/j.electacta.2010.02.012
19. W.Chen, X.He, Z.Jiang, B.Li, X.Li, L.LiN. *Chem. Eng. J*., **451**, 139071 (2023); https://doi.org/10.1016/j.cej.2022.139071
20. *Adsorbenty, ikh poluchenie, svoistva i primenenie. (Adsorbents, their Preparation, Properties and Applications)*. (Leningrad:Nauka, 1962)
21. K.Kinoshita. *Carbon: Electrochemical and Physicochemical Properties*. (New York: Wiley, 1988)
22. S.J.Gregg, K.S.W.Sing. *Adsorption, Surface Area and Porosity*.(New York: Academic Press, 1967)
23. M.R.Tarasevich. *Elektrokhimiya Uglerodnykh Materialov. (Electrochemistry of Carbon Materials)*. (Moscow: Nauka, 1984)
24. H.Xue, X.Gao, M.K.Seliem, M.Mobarak, R.Dong. *Chem. Eng. J*., **451**, 138735 (2023); https://doi.org/10.1016/j.cej.2022.138735
25. J.S.Mattson, H.B.Makr. *Activated Carbon*. (New York: Marcel Dekker, 1971)
26. I.A.Tarkovskaya. *Okislennyi Ugol' (Oxidized Coal)*. (Kiev: Naukova Dumka, 1981)
27. Y.Jiang, J.Li, Z.Jiang, M.Shi, R.Sheng, Z.Liu, S.Zhang. *Carbon*, **175**, 281 (2021); https://doi.org/10.1016/j.carbon.2021.01.016
28. Yu.M.Volfkovich, D.A.Bograchev, A.A.Mikhalin, V.S.Bagotsky. *J. Solid State Electrochem*., **18**, 1351 (2014); https://doi.org/10.1007/s10008-013-2271-4
29. A.Burke. *J. Power Sources*, **91**, 57 (2000); https://doi.org/10.1016/S0378-7753(00)00485-7
30. Yu.M.Volfkovich, T.M.Serdyuk. *Russ. J. Electrochem*., **38**, 935 (2002); https://doi.org/10.1023/A:1020220425954
31. A.G.Pandolfo, A.F.Hollenkamp. *J. Power Sources*, **157**, 11 (2006); https://doi.org/10.1016/j.jpowsour.2006.02.065
32. P.Sharma, T.S.Bhatti. *Energy Convers. Management*, **51**, 2901 (2010); https://doi.org/10.1016/j.enconman.2010.06.031
33. H.Chen, T.N.Cong, W.Yang, C.Tan, Y.Li, Y.Ding. *Prog. Nat. Sci*., **19**, 291 (2009); https://doi.org/10.1016/j.pnsc.2008.07.014
34. Yu.M.Volfkovich, V.M.Mazin, N.A.Urisson. *Russ. J. Electrochem*., **34**, 740 (1998); https://doi.org/10.1007/BF02252290
35. M.Inagaki, H.Konno, O.Tanaike. *J. Power Sources*, **195**, 7880 (2010); https://doi.org/10.1016/j.jpowsour.2010.06.036
36. A.Faisal, Al.Marzooqi, A.Amal, A.Ghaferi, I.Saadat, N.Hilal. *Desalination*, **342**, 3 (2014); https://doi.org/10.1016/j.desal.2014.02.031
37. M.Kim, X.Xu, R.Xin, J.Earnshaw, A.Ashok. *ACS Appl. Mater*., **13**, 52034 (2021); https://doi.org/10.1021/acsami.1c09107
38. Y.Oren. *Desalination*, **228**, 10 (2008); https://doi.org/10.1016/j.desal.2007.08.005
39. H.Strathmann. *Sustain. Sci. Eng*., **2**, 141 (2010); https://doi.org/10.1016/S1871-2711(09)00206-2

40. E.Avraham, M.Noked, Y.Bouhadana, A.Soffer, D.Aurbach. *J. Electrochem. Soc*., **156**, 157 (2009); https://doi.org/10.1149/1.3193709
41. M.E.Suss, T.F.Baumann, W.L.Bourcier, C.M.Spadaccini, K.A.Rose, J.G.Santiago, M.Stadermann. *Energy Environ. Sci*., **5**, 9511 (2012); https://doi.org/10.1039/c2ee21498a
42. R.A.Rica, R.Ziano, D.Salerno, F.Mantegazza, D.Brogioli. *Phys. Rev. Lett*., **109**, 1388 (2012); https://doi.org/10.1103/PhysRevLett.109.156103
43. P.Srimuk, F.Kaasik, B.Krüner, A.Tolosa, S.Fleischmann, N. Jäckel, M.C.Tekeli. *J. Mater. Chem. A*, **4** 18265 (2016); https://doi.org/10.1039/C6TA07833H
44. H.Zhang, J.Tian, X.Cui, J.Li, Z.Zhu. *Carbon*, **201**, 920 (2023); https://doi.org/10.1016/j.carbon.2022.10.002
45. Yu.M.Volfkovich, D.A.Bograchev, A.A.Mikhalin, A.Yu. Rychagov, V.E.Sosenkin, D.Park. *Desalination Water Treatment*, **69**, 130 (2017); https://doi.org/10.5004/dwt.2017.0469
46. G.M.Batyrin. *Vysokoporistye Uglerodnye Materialy*. (*Highly Porous Carbon Materials)*. (Moscow; Khimiya, 1976)
47. Yu.M.Volfkovich, A.A.Mikhalin, A.Yu.Rychagov, V.E.Sosenkin, D.A.Bograchev. *Russ. J. Electrochem*., **56**, 869 (2020); https://doi.org/10.1134/S1023193520100122
48. Yu.M.Volfkovich, V.S.Bagotzky. *J. Power Sources*, **48**, 339 (1994); https://doi.org/10.1016/0378-7753(94)80030-8
49. Yu.M.Volfkovich, V.S.Bagotzky, V.E.Sosenkin, I.A.Blinov. *Colloid Surf., A: Physicochem. Eng. Aspects*, **187**–**188**, 349 (2001); https://doi.org/10.1016/S0927-7757(01)00650-1
50. Yu.M.Volfkovich, A.N.Filippov, V.S.Bagotsky. *Structural Properties of Porous Materials and Powders Used in Different Fields of Science and Technology*. (London: Springer, 2014)
51. Yu.M.Volfkovich, A.V.Sakars, A.A.Volinsky. *Int. J. Nanotechnol*., **2**, 292 (2005); https://doi.org/10.1504/IJNT.2005.008066
52. J.Rouquerol, G.Baron, R.Denoyel, H.Giesche, J.Groen, P.Klobes, P.Levitz, A.V.Neimark, S.Rigby, R.Skudas, K.Sing, M.Thommes, K.Unger. *Pure Appl. Chem*., **84**, 107 (2012); https://doi.org/10.1351/PAC-REP-10-11-19
53. K.Xia, Q.Gao, J.Jiang, J.Hu. *Carbon*, **46**, 1718 (2008); https://doi.org/10.1016/j.carbon.2008.07.018
54. H.Xu, L.Wang, Y.Zhang, Y.Chen, S.Gao. *Nanoscale*, **13**, 10051 (2021); https://doi.org/10.1039/D1NR01640G
55. Z.Tang, X.Li, T.Sun, S.Shen, X.Huixin, J.Yang. *Microporous Mesoporous Mater*., **272**, 40 (2018); https://doi.org/10.1016/j.micromeso.2018.06.020
56. Y.Zhou, X.Ren, Y.Du, Y.Jiang, J. Wan, F.Ma. *Electrochim. Acta*, **355**, 136801 (2020); https://doi.org/10.1016/j.electacta.2020.136801
57. W.Xing, C.C.Huang, S.P.Zhuo, X.Yuan, G.Q.Wang. *Carbon*, 47, 1715 (2009); https://doi.org/10.1016/j.carbon.2009.02.024
58. X.Yang, S.Zhao, Z.Zhang, Y.Chi, C.Yang. *J. Colloid Interface Sci.*, 614, 298 (2022); https://doi.org/10.1016/j.jcis.2022.01.093
59. Z.Li, A.Cheng, W.Zhong, H.Ma, M.Si, X.Ye, Z.Li. *Microporous Mesoporous Mater*., **306**, 110440 (2020); https://doi.org/10.1016/j.micromeso.2020.110440
60. J.Kim, J.H.Eum, J.Kang, O.Kwon, H.Kim, D.W.Kim. *Sci. Rep*., **11**, 2063 (2021); https://doi.org/10.1038/s41598-020-80518-4
61. X.Zhang, H.Zhang, C.Li, K.Wang, X.Sun, Y.Ma. *RSC Adv*., 4, 45862 (2014); https://doi.org/10.1039/C4RA07869A
62. H.Chen, D.Liu, Z.Shen, B.Bao, S.Zhao, L.Wu. *Electrochim. Acta*, **180**, 241 (2015); https://doi.org/10.1016/j.electacta.2015.08.133
63. Yu.M.Volfkovich, A.Yu.Rychagov, V.E.Sosenkin. *Russ. J. Electrochem*., **58**, 730 (2022); https://doi.org/10.1134/S1023193522090142
64. B.Chang, H.Yin, X.Zhang, S.Zhang, B.Yang. *Chem. Eng. J*., **312**, 191 (2017); https://doi.org/10.1016/j.cej.2016.11.129
65. E.J.Lee, L.Lee, M.A.Abbas, J.H.Bang. *Phys. Chem*., **19**, 21140 (2017); https://doi.org/10.1039/C7CP03546B
66. X.Luo, X.Chen, Y.Mo. *New Carbon Mater*., **36**, 49 (2021); https://doi.org/10.1016/S1872-5805(21)60004-5
67. X.Zhang, H.Li, K.Zhang, Q. Wang, B. Qin. *J. Electrochem. Soc*., **165**, A2084 (2018); https://doi.org/10.1149/2.0491910jes
68. L.Xie, F.Su, L.Xie, X.Guo, Z.Wang, Q.Kong. *Mater. Chem. Front*., **4**, 2610 (2020); https://doi.org/10.1039/D0QM00180E
69. Y.J.Heo, H.I.Lee, J.W.Lee, M.Park, K.Y.Rhee. *Composites, Part B: Eng*., **161**, 10 (2019); https://doi.org/10.1016/j.compositesb.2018.10.026
70. Z.Lin, X.Xiang, S.Peng, X.Jiang, L.Hou. *J. Electroanal. Chem*., **823**, 563 (2018); https://doi.org/10.1016/j.jelechem.2018.06.031
71. C.Long, L.Jiang, X.Wu, Y.Jiang, D.Yang, C.Wang. *Carbon*, **93**, 412 (2015); https://doi.org/10.1016/j.carbon.2015.05.040
72. T.Y.Kim, G.Jung, S.Yoo, K.S.Suh, R.S.Ruoff. *ACS Nano*, **7**, 6899 (2013); https://doi.org/10.1021/nn402077v
73. P.Hao, Z.Zhao, J.Tian, H.Li, Y.Sang, G.Yu, H.Cai, H.Liu. *Nanoscale*, **6**, 12120 (2014); https://doi.org/10.1039/C4NR03574G
74. T.Shimizu, K.Kobashi, H. Nakajima. *ACS Appl. Energy Mater*., **4**, 9712 (2021); https://doi.org/10.1021/acsaem.1c01802
75. R.A.Fisher, M.R.Watt, W.J.Ready. *J. Solid State Sci. Technol*., **2**, 2 M3170 *(*2013); https://doi.org/10.1149/2.017310jss
76. Y.Zhang, H.Chen, S.Wang, X.Zhao, F.Kong. *Microporous Mesoporous Mater*., **297**, 110032 (2020); https://doi.org/10.1016/j.micromeso.2020.110032
77. X.Liu, S.Li, R.Mi, J.Mei, L.M.Liu, L.Cao, W.M.Lau, H.Liu. *Appl.Energy*, **153**, 32 (2015); https://doi.org/10.1016/j.apenergy.2015.01.141
78. Yu.M.Volfkovich, A.A.Mikhalin, A.Yu.Rychagov. *Russ. J. Electrochem*., **49**, 594 (2013); https://doi.org/10.1134/S1023193513060141
79. S.L.Goertzen, K.D.Theriault, A.M.Oickle, A.C.Tarasuk, H.A.Andreas. *Carbon*, **48**, 1252 (2010); https://doi.org/10.1016/j.carbon.2009.11.050
80. A.M.Oickle, S.L.Goertzen, K.R.Hopper, Y.O.Abdalla, H.A.Andreas. *Carbon*, **48**, 3313 (2010); https://doi.org/10.1016/j.carbon.2010.05.004
81. Yu.M.Volfkovich, I.V.Goroncharovskaya, A.K.Evseev, V.E.Sosenkin, M.M.Gol'din. *Russ. J. Electrochem*., **53**, 1363 (2017); https://doi.org/10.1134/S1023193517120126
82. D.A.Fridrikhsberg. In *Electrokineticheskie Svoistva Kapillyarnykh Sistem.* (*Electrokinetic Properties of Capillary Systems)*. (Moscow: Isd. AH SSSR, 1956). P. 156
83. Yu.M.Volfkovich, A.Yu.Rychagov, A.A.Mikhalin, M.M.Kardash, N.A.Kononenko, D.V.Ainetdinov, S.A.Shkirskaya, V.E.Sosenkin. *Desalination*, **426**, 1 (2018); https://doi.org/10.1016/j.desal.2017.10.035
84. B.B.Damaskin, O.A.Petrii, G.A.Tsirlina. *Elektrokhimiya*. (*Electrochemistry)*, (Moscow: Khimiya, 2008)
85. J.L.Figueiredo, M.F.R.Pereira, M.M.A.Freitas, J.J.M.O´rfao. *Carbon*, **37**, 1379 (1999); https://doi.org/10.1016/S0008-6223(98)00333-9
86. B.Conway. *Electrochemical Supercapacitors: Scientific Fundamentals and Technological Applications*. (Berlin: Springer, 2013)
87. V.S.Bagotsky, A.M.Skundin, Yu.M.Volfkovich. *Electrochemical Power Sources. Batteries, Fuel Cells, Supercapacitors*. (New York: Wiley, 2015)
88. Yu.M.Volfkovich. *Russ. Chem. Rev*., **91**, RCR5044 (2022); https://doi.org/10.1070/RCR5044
89. Yu.M.Volfkovich, D.A.Bograchev, A.Yu.Rychagov, V.E.Sosenkin, M.Yu.Chaika. *Solid State Electrochem*., **19**, 1 (2015); https://doi.org/10.1007/s10008-014-2581-1
90. D.A.Bograchev, D.Yu.Gryzlov, V.E.Sosenkin, Yu.M.Volfkovich.*Electrochim. Acta*, **319**, 552 (2019); https://doi.org/10.1016/j.electacta.2019.07.002
91. Z.Algharaibeh, P.G.Pickup. *Electrochem. Commun.*, **13**, 147 (2011); https://doi.org/10.1016/j.elecom.2010.11.036
92. B.Z.Jang, C.Liu, D.Neff, Z.Yu, M.C.Wang, W.Xiong, R.Zhamu. *Nano Lett*., **11**, 3785 (2011); https://doi.org/10.1021/nl2018492

93. A.S.Solyanikova, M.Yu.Chayka, V.A.Parfenov, S.D.Kirik, T.A.Kravchenko. *Russ. J. Electrochem*., **51**, 764 (2015); https://doi.org/10.1134/S1023193515080091
94. D.Sui, L.Si, C.Li, Y.Yang, Y.Zhang, W.Yan. *Chemistry*, **3**, 1215 (2021); https://doi.org/10.3390/chemistry3040089
95. P.Jeżowski, O.Crosnier, E.Deunf, P.Poizot, F.Béguin, F.Brousse. *Nat. Mater*., **17**, 167 (2018); https://doi.org/10.1038/nmat5029
96. G.Li, Z.Yang, Z.Yin, H.Guo, Z.Wang, G.Yan. *J. Mater. Chem*., **7**, 15541 (2019); https://doi.org/10.1039/C9TA01246J
97. P.Kurzweil, M.Shamonin. *Batteries*, **4**, 35 (2018); https://doi.org/10.3390/batteries4030035
98. K.Liu, C.Yu, W. Guo, L.Ni, J. Yu, Y.Xie, Z.Wang. *J. En*ergy, **58**, 94 (2021); https://doi.org/10.1016/j.jechem.2020.09.041
99. M.O.Bamgbopa, D.Belaineh, D.A.Mengistie, J.Edberg, I. Engquist, M.Berggren, K.Tybrandt. *J. Mater. Chem. A*, **9**, 2184 (2021); https://doi.org/10.1039/D0TA09429C
100. H.Wang, Q.Zhou, D.Yao, H.Ma. *Adv. Mater. Interfaces*, **5**, 1701547 (2018); https://doi.org/10.1002/admi.201701547
101. M.Ceraolo, G.Lutzemberger. *J. Energy Storage*, **11**, 211 (2017); https://doi.org/10.1016/j.est.2017.03.001
102. M.A.Davis, H.A.Andreas. *Carbon*, **139**, 299 (2018); https://doi.org/10.1016/j.carbon.2018.06.065
103. A.M.Oickle, J.Tom, H.A.Andreas. *Carbon*, **110**, 232 (2016); https://doi.org/10.1016/j.carbon.2016.09.011
104. O.Okhay A.Tkach, P.Staiti, F.Lufrano. *Electrochim. Acta*, **353**, 136540 (2020); https://doi.org/10.1016/j.electacta.2020.136540
105. T.Yumak, D.Bragg, E.M.Sabolsky. *Appl. Surface Sci*., **469**, 983 (2019); https://doi.org/10.1016/j.apsusc.2018.09.079
106. M.Xia, J.Nie, Z.Zhang, X.Lu, Z.L.Wang. *Nano Energy*, **47**, 43 (2018); https://doi.org/10.1016/j.nanoen.2018.02.022
107. H.Miniguano, A.Barrado, C.Fernández, P.Zumel, A.Lázaro. *Energies*, **12**, 1 (2019); https://doi.org/10.3390/en12091776
108. S.Subramanian, M.A.Johny, M.M.Neelanchery, S.Ansari. *IEEE Transact. Power Electron*., **33**, 10410 (2018); https://doi.org/10.1109/TPEL.2018.2810889
109. S.Satpathy, M.Dhar, B.K.Bhattacharyya. *J. Energy Storage*, **31**, 101606 (2020); https://doi.org/10.1016/j.est.2020.101606
110. T.Ghanbari, E.Moshksar, S.Hamedi, F.Rezaei, Z.Hosseini. *J. Power Sources*, **495**, 229787 (2021); https://doi.org/10.1016/j.jpowsour.2021.229787
111. M.Haque, Q.Li, A.D.Smith, V.Kuzmenko. *J. Power Sources*, **453**, 227897 (2020); https://doi.org/10.1016/j.jpowsour.2020.227897
112. M.Liu, M.Xia, R.Qi, Q.Ma, M.Zhao, Z.Zhang. *ChemElectrochem*, **6**, 2531 (2019); https://doi.org/10.1002/celc.201900173
113. J.Chung, H.Park, C.Jung. *Electrochim. Acta*, **369**, 137698 (2021); https://doi.org/10.1016/j.electacta.2020.137698
114. K.Ge, G.Liu. *Chem. Commun*, **55**, 7167 (2019); https://doi.org/10.1039/C9CC02424G
115. R.K.Mishra, G.J.Choi, Y.Sohn, S.H.Lee, J.S.Gwag. *Mater. Lett*., **253**, 250 (2019); https://doi.org/10.1016/j.matlet.2019.06.073
116. A.J.Paleo, P.Stait, A.Brigandì, F.N.Ferreira, A.M.Rocha, F.Lufrano. *Energy Storage Mater*., **12**, 204 (2018); https://doi.org/10.1016/j.ensm.2017.12.013
117. M.G.Hosseini, H.Rasouli, E.Shahryari, L.Naji. *J. Appl. Polym. Sci*., **13**, 44926 (2017); https://doi.org/10.1002/app.44926
118. A.A.Łatoszynska, P.Taberna, P.Simon, W.Wieczorek. *Electrochim*. *Acta*, **242**, 31 (2017); https://doi.org/10.1016/j.electacta.2017.04.122
119. J.Li, J.Qiao, K.Lian. *Energy Storage Mater*., **24**, 6 (2020); https://doi.org/10.1016/j.ensm.2019.08.012
120. K.Liu, C.Yu, W. Guo, L.Ni, J. Yu, Y.Xie. *J. Energy. Chem*., **58**, 94 (2021); https://doi.org/10.1016/j.jechem.2020.09.041
121. J.F.Shen, Y.J.He, Z.F.Ma. *J. Power Sources*, **303**, 294 (2016); https://doi.org/10.1016/j.jpowsour.2015.11.001
122. Yu.M.Volfkovich, A.Yu.Rychagov, A.A.Mikhalin, A.A.Sosenkin, E.N.Kabachkov, Yu.M.Shulga, A. Michtchenko. *J. Electroanal. Chem*., **910**, 116198 (2022); https://doi.org/10.1016/j.jelechem.2022.116198
123. Yu.M.Shulga, S.A.Baskakov, Yu.V.Baskakova, A.S.Lobach, E.N.Kabachkov, Yu.M.Volfkovich, V.E.Sosenkin, N.Yu. Shulga, S.I.Nefedkin, Y.Kumar, A. Michtchenko. *J. Alloys Compd*., **730**, 88 (2018); https://doi.org/10.1016/j.jallcom.2017.09.249
124. Yu.M.Shulga, S.A.Baskakov, Yu.V.Baskakova, A.S.Lobach, Yu.M.Volfkovich, V.E.Sosenkin, N.Yu.Shulga, Y.N.Parkhomenko, A.Michtchenko, Y.Kumar. *Microporous Mesoporous Mater*., **245**, 24 (2017); https://doi.org/10.1016/j.micromeso.2017.02.061
125. Y.J.Hsiao, L.Y.Lin. *ACS Sustain. Chem. Eng*., **8**, 2453 (2020); https://doi.org/10.1021/acssuschemeng.9b06569
126. J.Xiao, R.Momen, C.Liu. *Electrochem. Commun*., **132**, 107143 (2021); https://doi.org/10.1016/j.elecom.2021.107143
127. S.Lee, G.H.An. *J. Energy Chem*., **68**, 1 (2022); https://doi.org/10.1016/j.jechem.2021.11.008
128. Yi.Wang, Yue Wang, G.Q.Huang, C.Lin. *Eur. J. Operational*., **24** (2023); https://doi.org/10.1016/j.ejor.2023.03.028
129. Y.He, Y.Zhang, X.Li, Z.Lv, X.Wang, Z.Liu, X.Huang. *Electrochim. Acta*, **282**, 618 (2018); https://doi.org/10.1016/j.electacta.2018.06.103
130. X.Li, Y.Jiang, P.Wang, Y.Mo, Z.Li, R.Yu, Y.Du. *New Carbon Mater*., **35**, 232 (2020); https://doi.org/10.1016/S1872-5805(20)60487-5
131. S.Xu, J.Lu, S.Zou, S.Shi, P.He, H.Zhang, S.Kang. *Energy Fuels*, **35**, 5298 (2021); https://doi.org/10.1021/acs.energyfuels.0c03992
132. Z.Wang, P.Zheng, J.Guo. *Appl. Phys. A*, **127**, 323 (2021); https://doi.org/10.1007/s00339-021-04356-5
133. S.Lin, J.Tang, K.Zhang, Y.Chen, R.Gao, H.Yin. *Nanoscale Adv.*, **5**, 1163 (2023); https://doi.org/10.1039/D2NA00506A
134. A.Ilnicka, M.Skorupska, M.Szkoda, Z.Zarach. *Sci. Rep*., **11**, 18387 (2021); https://doi.org/10.1038/s41598-021-86507-5
135. Y.Wang, X.Wang, X.Li, X.Li, Y.Liu, Y.Bai. *Adv. Funct. Mater*., **31**, 2008185 (2021); https://doi.org/10.1002/adfm.202008185
136. R.Vinodh, Y.Sasikumar, H.J.Kim, R.Atchudan. *J. Industr. Eng.Chem*., **104**, 155 (2021); https://doi.org/10.1016/j.jiec.2021.08.019
137. H.Wang, X.Chen, J.Zhang, Z.Yuan, P.Ye, J.Shen. *Appl. Surface Sci*., **598**, 153819 (2022); https://doi.org/10.1016/j.apsusc.2022.153819
138. Y.Liu, H.Wang, C.Li, S.Wang, L.Li. *Int. J. Energy Res*., **46**, 370 (2022); https://doi.org/10.1111/1468-2427.13085
139. R.Peng, K.Han, K.Tang. *J. Electrochem. Soc*., **169**, 060523 (2022); https://doi.org/10.1149/1945-7111/ac72ca
140. R.Wang, H.Wang, Y.Zhou, Z.Gao, Y.Han. *Inorg. Chem. Front*., **9**, 2530 (2022); https://doi.org/10.1039/D2QI00017B
141. Y.Lian, H.Chen, Z.Cao, J.Sun, J.Zhao, H.Zhang. *Desalination*, **532**, 115758 (2022); https://doi.org/10.1016/j.desal.2022.115758
142. N.Singh, A.Malik, S.Nohwar, R.Jana. *New J. Chem*., **47**, 5308 (2023); https://doi.org/10.1039/D2NJ05566J
143. Y.Zheng, K.Chen, K.Jiang, F.Zhang, G.Zhu. *J. Energy Storage*, **56**, 105995 (2022); https://doi.org/10.1016/j.est.2022.105995
144. L.Chen, Z.Ji, G.Tang, J.Zhong, G.Zhu, A.Yuan. *Chem. Eng. J*., **456**, 141166 (2023); https://doi.org/10.1016/j.cej.2022.141166
145. Yu.M.Volfkovich. *Russ. J. Electrochem*., **56**, 18 (2020); https://doi.org/10.1134/S1023193520010097
146. Y.Cai, Y.Wang, R.Fang, J.Wang. *Separation and Purification Technology*, **280**, 119828 (2022); https://doi.org/10.1016/j.seppur.2021.119828
147. H.Strathmann. *Sustainability Scienceand Engineering*., **2**, 141, (2010); https://doi.10.1016/S1871-2711(09)00206-2

148. A.Soffer, M.Folman. *J. Electroanal. Chem*., **38**, 25 (1972); https://doi.org/10.1016/S0022-0728(72)80087-1
149. Z.Ding, X.Xu, J.Li, Y.Li, K.Wang, T.Lu. *Chem. Eng. J*., **430** 133161 (2022); https://doi.org/10.1016/j.cej.2021.133161
150. Z.Chen, X.Xu, Y.Liu, J.Li, K.Wang, Z.Ding, F.Meng, T.Lu. *Desalination*, **528**, 115616 (2022); https://doi.org/10.1016/j.desal.2022.115616
151. Y.A.Jande, W.S.Kim. *Desalination*, **329**, 29 (2013); https://doi.org/10.1016/j.desal.2013.08.023
152. H.Jiang, J.Zhang, K.Luo, W.Xing, J.Du, Y.Dong. *Sci. Total Environ.*, **804**, 150166 (2022); https://doi.org/10.1016/j.scitotenv.2021.150166
153. X.Ma, H.Wang, Q.Wu, J.Zhang, D.Liang, S.Lu, Y.Xiang. *J. Electrochem. Soc*., **166**, A236 (2019); https://doi.org/10.1149/2.0831902jes
154. R.Zhao, S.Porada, P.M.Biesheuvel, A.van der Wal. *Desalinatio*, **330**, 35 (2013); https://doi.org/10.1016/j.desal.2013.08.017
155. M.Andelman. *Separat. Purificat. Technol*., **80**, 262 (2011); https://doi.org/10.1016/j.seppur.2011.05.004
156. K.Wang, Y.Liu, Z.Ding, Z.Chen, X.Xu, M.Wang. *Chem. Eng. J*., **433**, 133578 (2022); https://doi.org/10.1016/j.desal.2021.115420
157. H.Li, I.Zou. *Desalination*, **275**, 62 (2011); https://doi.org/10.1016/j.desal.2011.02.027
158. P.M.Biesheuvel, R.Zhao, S.Porada, A.van der Wal. *J. Colloid Interface Sci*., **360**, 239 (2011); https://doi.org/10.1016/j.jcis.2011.04.049
159. R.Zhao, O. Satpradit, H.M.Rijnaarts, P.M.Biesheuvel, A.van der Wal. *Water Res*., **147**, 1941 (2013); https://doi.org/10.1016/j.watres.2013.01.025
160. P.M.Biesheuvel, A.van der Wal. *J. Membr. Sci*., **346**, 256 (2010); https://doi.org/10.1016/j.memsci.2009.09.043
161. A.G.El-Deen, J.H.Choi, C.S.Kima, K.Abdelrazek, K.A.Khali, A.A.Almajid, N.A.Barakat. *Desalination*, **61**, 53 (2015); https://doi.org/10.1016/j.desal.2015.01.033
162. X.Gao, A.Omosebi, N.Holubowitch, A.Liua, K.Ruha, J.Landon, K.Liu. *Desalination*, **399**, 16 (2016); https://doi.org/10.1016/j.desal.2016.08.006
163. Y.Zhao, Y.Wang, R.Wang, Y.Wu, S.Xu, J.Wang. *Desalination*, **330**, 35 (2013); https://doi.org/10.1016/j.desal.2013.08.017
164. Z.Wang, H.Gong, Y.Zhang, P.Liang, K.Wang. *Chem. Eng. J*., **316**, 1 (2017); https://doi: 10.1016/j.cej.2017.01.082
165. K.Singha, S.Poradab, H.D.de Gierb, P.M.Biesheuvel, L.C.de Smeta. *Desalination*, **455**, 115 (2019); https://doi.org/10.1016/j.desal.2018.12.015
166. J.Kang, T.Kima, T.Shin, J.Lee, J.-I.Ha, J.Yoon. *Desalination*, **398**, 144 (2016); https://doi.org/10.1016/j.desal.2016.07.025
167. J.E.Dykstra, R.Zhao, P.M.Biesheuvel, A. van der Wal. *Water Res*., **88**, 358 (2016); https://doi.org/10.1016/j.watres.2015.10.006
168. Y.Bian, P.Liang, X.Yang, X.Jiang, C.Zhang, X.Huang. *Desalination*, **381**, 95 (2016); https://doi.org/10.1016/j.desal.2015.11.016
169. J.E.Dykstra, K.J.Keesman, P.M.Biesheuvel, A. van der Wal. *Water Res*., **119**, 178 (2017); https://doi.org/10.1016/j.watres.2017.04.039
170. J.J.Lado, L.Rafael, R.L.Zornitta, F.A.Calvi, M.I.Tejedor-Tejedor, Anderson, L.A.M.Ruotolo. *J. Anal. Appl. Pyrol*., **126**, 143 (2017); https://doi.org/10.1016/j.jaap.2017.06.014
171. W.Tang, D.He, C.Zhang, P.Kovalsky, T.D.Waite. *Water Res*., **120**, 229 (2017); https://doi.org/10.1016/j.watres.2017.05.009
172. Yu.M.Volfkovich, N.A.Kononenko, A.A.Mikhalin, M.M.Kardash, A.Yu.Rychagov, S.V.Tsipliaev, S.A.Shkirskaya, V.E.Sosenkin.*Desalination Water Treatment*, **182**, 77 (2020); https://doi.org/10.5004/dwt.2020.25410
173. Yu.M.Volfkovich, A.A.Mikhalin, A.Yu.Rychagov, M.M.Kardash. *Protect. Met. Phys. Chem. Surfaces*, **57**, 68 (2021); https://doi.org/10.1134/S2070205121010214
174. Yu.M.Volfkovich, D.A.Bograchev, A.A.Mikhalin, A.Yu. Rychagov, V.E.Sosenkin, V.V.Milyutin, D.Park. In *Electrodes Based on Carbon Nanomaterials: Structure, Properties and Application to Capacitive Deionization in Static Cells*. (Shpringer, 2018). P. 127; https://doi.10.1007/978-3-319-91083-3_9
175. Yu.M.Volfkovich, D.A.Bograchev, A.A.Mikhalin, A.Yu. Rychagov, V.E.Sosenkin, D.Park. *Desalination Water Treatment*, **69**, 130 (2017); https://doi.org/10.5004/dwt.2017.0469
176. M.Ćalasan, S.H.Aleem, H.M.Hasanien, Z.M.Alaas. *Energy*, **264**, 126165 (2023); https://doi.org/10.1016/j.energy.2022.126165
177. F.Darıcık, A.Topcu, K.Aydın, S.Çelik. *Intern. J. Hydrogen Energy*, **48**, 1090 (2023); https://doi.org/10.1016/j.ijhydene.2022.09.297
178. *Hanbook of Fuel Cells. Fundamentals Technology and Applications*. (Eds W.Vielstich, A.Lamm, H.A.Gasteiger). (Chichester: Wiley, 2003)
179. V.S.Bagotsky. *Fuel Cells: Problems and Solutions*. (Hoboken, NJ: Wiley, 2009)
180. S.Gottesfeld, T.A.Zawodzinski. In *Advances in Electrochemical Science and Engineering. Vol. 5*. (Eds R.C.Alkire, H.Gerischer, D.M.Kolb, C.W.Tobias). (Weinheim: Wiley-VCH, 1997). P. 195
181. Yu.M.Volfkovich, V.E.Sosenkin, N.F.Nikolskaya. *Russ. J. Electrochem*., **46**, 410 (2010); https://doi.10.31857/S0424857023050043